Received November 11, 2015, accepted November 27, 2015. Date of publication xxxx 00, 0000, date of current version xxxx 00, 0000.

Digital Object Identifier 10.1109/ACCESS.2015.2505676

Compressed Impairment Sensing-Assisted and Interleaved-Double-FFT-Aided Modulation Improves Broadband Power Line Communications Subjected to Asynchronous Impulsive Noise

HONGMING ZHANG, (Student Member, IEEE), LIE-LIANG YANG, (Fellow, IEEE), AND LAJOS HANZO, (Fellow, IEEE)

School of Electronics and Computer Science, University of Southampton, Southampton SO17 1BJ, U.K.

Corresponding author: L. Hanzo (lh@ecs.soton.ac.uk)

This work was supported by the European Research Council Advance Fellow Grant.

ABSTRACT In power line communications (PLCs), the multipath-induced dispersion and the impulsive noise are the two fundamental impediments in the way of high-integrity communications. The conventional orthogonal frequency-division multiplexing (OFDM) system is capable of mitigating the multipath effects in PLCs, but it fails to suppress the impulsive noise effects. Therefore, in order to mitigate both the multipath effects and the impulsive effects in PLCs, in this paper, a compressed impairment sensing (CIS)-assisted and interleaved-double-FFT (IDFFT)-aided system is proposed for indoor broadband PLC. Similar to classic OFDM, data symbols are transmitted in the time-domain, while the equalization process is employed in the frequency domain in order to achieve the maximum attainable multipath diversity gain. In addition, a specifically designed interleaver is employed in the frequency domain in order to mitigate the impulsive noise effects, which relies on the principles of compressive sensing (CS). Specifically, by taking advantage of the interleaving process, the impairment impulsive samples can be estimated by exploiting the principle of CS and then cancelled. In order to improve the estimation performance of CS, we propose a beneficial pilot design complemented by a pilot insertion scheme. Finally, a CIS-assisted detector is proposed for the IDFFT system advocated. Our simulation results show that the proposed CIS-assisted IDFFT system is capable of achieving a significantly improved performance compared with the conventional OFDM. Furthermore, the tradeoffs to be struck in the design of the CIS-assisted IDFFT system are also studied.

INDEX TERMS Power line communications, OFDM, impulsive noise, compressed sensing.

NOMENCLATURE

2D	Two-Dimensional
BB-PLC	BroadBand Power Line Communication
BER	Bit Error Ratio
CCDF	Complementary Cumulative Distribution Function
CIS	Compressed Impairment Sensing
CP	Cyclic Prefix
CS	Compressed Sensing
CTF	Channel Transfer Function
DFT	Discrete Fourier Transform
ETF	Equiangular Tight Frame
FD	Frequency-Domain
FDCHTF	Frequency-Domain CHannel Transfer Factor
FFT	Fast Fourier Transform
IDFFT	Interleaved-Double-FFT
IFDMA	Interleaved Frequency Division Multiple Access
IFFT	Inverse Fast Fourier Transform
ISI	Inter-Symbol Interference
MAP	Maximum *A Posterior*
MIP	Mutual Incoherence Property
ML	Maximum-Likelihood
MMSE	Minimum Mean Square Error
MWBE	Maximum-Welch-Bound-Equality

OFDM	Orthogonal Frequency-Division Multiplexing
PAPR	Peak-to-Average Power Ratio
PLC	Power Line Communication
PSD	Power Spectral Density
QAM	Quadrature Amplitude Modulation
QoS	Quality-of-Services
QPSK	Quadrature Phase-Shift Keying
RIP	Restricted Isometry Property
SINR	Signal to Interference plus Noise power Ratio
SNR	Signal-to-background Noise power Ratio
TD	Time-Domain

NOTATIONS

$(\cdot)^T$ and $(\cdot)^*$	the transpose and the conjugate, respectively
$(\cdot)^H$ and $(\cdot)^{-1}$	the conjugate transpose and the inverse, respectively
$\mathbb{E}[\cdot]$	the expectation operator
$\mathbb{C}^{M\times L}$	the set of $(M \times L)$-element matrices in the complex field
$\boldsymbol{x}$ and $\boldsymbol{X}$	vector in boldface lower-case and matrix in boldface upper-case, respectively
$\boldsymbol{x}(l)$ and $x(m, l)$	lth block of symbols and mth symbol of lth block, respectively
$\boldsymbol{I}_M$	the $(M \times M)$-element identity matrix
$\boldsymbol{\Theta}_i$	the $(M \times M_i)$-element mapping matrix whose columns are extracted from the $\boldsymbol{I}_M$ according to an index set $\mathcal{I}_i$
$\boldsymbol{\mathcal{F}}_M$	the normalized $(M \times M)$-element DFT matrix, which satisfies $\boldsymbol{\mathcal{F}}_M\boldsymbol{\mathcal{F}}_M^H = \boldsymbol{\mathcal{F}}_M^H\boldsymbol{\mathcal{F}}_M = \boldsymbol{I}_M$
$diag\{\boldsymbol{x}\}$	the diagonal matrix with elements in $\boldsymbol{x}$ on its diagonal
$Card(\mathcal{I})$	the cardinality of a set $\mathcal{I}$
$Supp(\boldsymbol{x})$	the support of a vector $\boldsymbol{x}$, which is defined as the set containing the indices of the non-zero elements of $\boldsymbol{x}$
$\|\boldsymbol{x}\|_p$	the ℓ_p-norm of a vector $\boldsymbol{x}$, where $p > 0$
$\|\boldsymbol{x}\|_0$	the pseudo-ℓ_0-norm of a vector $\boldsymbol{x}$, which is defined as $\|\boldsymbol{x}\|_0 = Card(Supp(\boldsymbol{x}))$
$\{A\}\backslash\{B\}$	the difference of two sets $\{A\}$ and $\{B\}$

I. INTRODUCTION

Power line communication (PLC) is expected to play an important role in meeting the dramatic teletraffic increase of telecommunications in the next decade [1]. The main advantage of PLC is its cost-efficiency, which is due to the fact that it relies on the existing grid structure. However, the electrical supply networks have not been designed for data transmissions, hence they constitute a hostile propagation environment [2] and there are still a lot of challenges to be tackled. Specifically, the signals transmitted over power line channels experience both propagation path-loss, as well as multipath propagation and impulsive noise. The path-loss encountered in PLC is the result of the skin effect and dielectric losses [3]. By contrast, the dispersive multipath propagation experienced in PLC is caused by the impedance mismatch between the transmitter and its corresponding receiver [4]. Due to the multipath propagation, a transmitted symbol may be spread over several adjacent symbols at the receiver, hence generating inter-symbol interference (ISI), as detailed in [4]. Measurement results show that the coherence bandwidth of indoor PLC channels is typically 50 kHz to 500 kHz, which is much lower than its total transmission bandwidth. Thus, the PLC channels are usually frequency-selective. Furthermore, the authors of [2] show that the time variation of the PLC channel parameters can be classified into two types, namely into short-term and long-term variations. The long-term variation is usually caused by the switching events experienced in PLC networks, which can be assumed to be time-invariant within a duration of a few seconds. By contrast, the short-term variation is mainly due to the fact that many electrical devices exhibit characteristics that are dependent on the mains frequency [5], which can be assumed to be time-invariant within hundreds of microseconds. Consequently, the latter type of variation is cyclic, and the channel parameters are usually periodical in time. Owing to the above characteristics, the PLC channels are typically slowly time-varying. The statistical characterisations of indoor PLC channels can be found in [6].

On the other hand, in PLC, the noise can usually be classified into two categories: background noise and impulsive noise [7], [8]. The impulsive noise is typically characterized by the duration, inter-arrival time and power of its components [7]. According to its behavior with respect to the mains cycle, impulsive noise can be classified into three types, namely periodic mains-synchronous impulsive noise, periodic impulsive noise that is asynchronous with the mains, as well as asynchronous impulsive noise [7]. Typically, the asynchronous impulsive noise, which is mainly caused by the connection and disconnection of electrical devices, is the major impairment of broadband PLC (BB-PLC) due to its high power and unpredictable nature. Therefore, we focus our attention on the mitigation of asynchronous impulsive noise. The measurement results of [7]–[9] have shown that the asynchronous impulsive noise bursts experienced in PLC are relatively long in comparison to those in wireless communications. More specifically, the measurement results of [7] showed that the average duration of the asynchronous impulsive noise bursts in PLC varies between microseconds and milliseconds. By contrast, in wireless communications, the duration of impulsive noise bursts is usually less than 0.1 μs [10]. These observations in turn imply that if signal samples with a symbol-duration of say 10 ns are transmitted at a Nyquist-rate of 100 MBaud, then 10^3 successive symbols may be corrupted by an impulsive noise burst, once it occurs. By contrast, at the typical wireless communications band-rate of say 1 MBaud, no more than

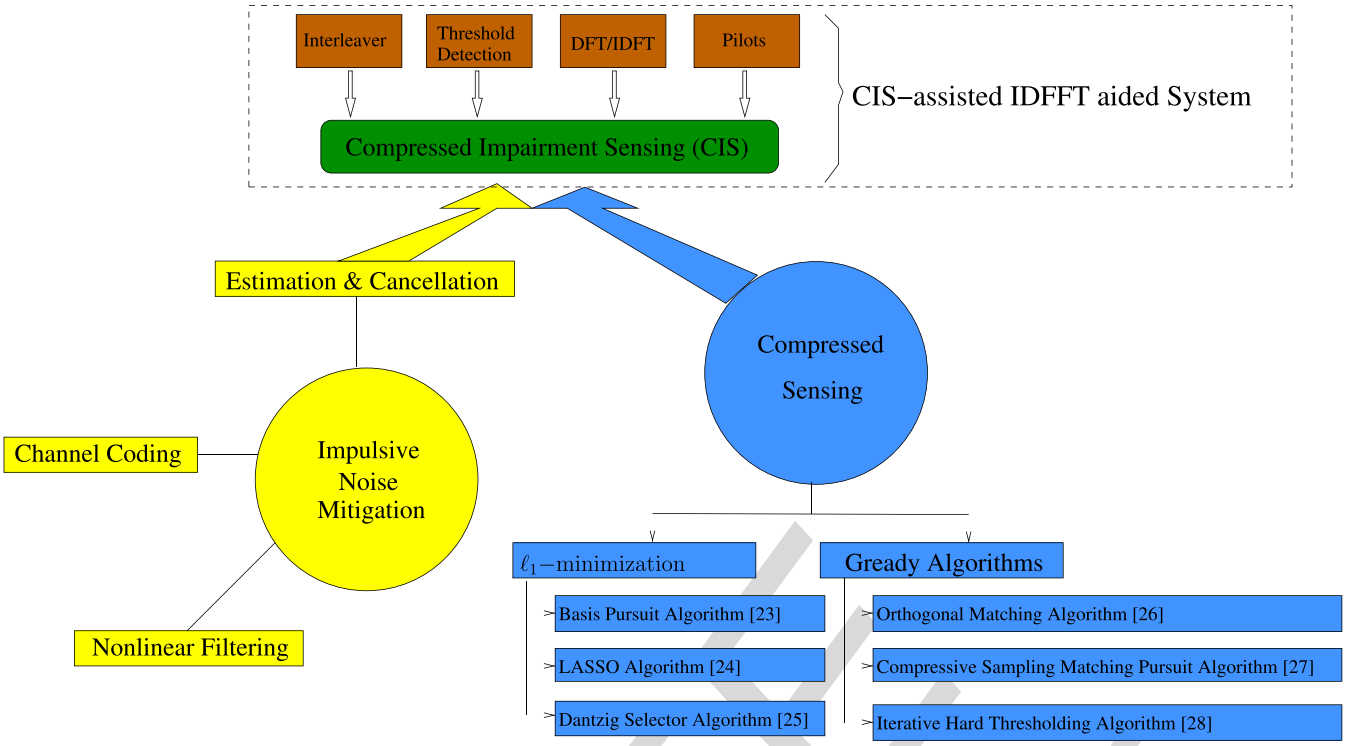

FIGURE 1. **Illustration of the relationships between compressed sensing (CS), impulsive noise mitigation as well as compressed impairment sensing (CIS). Explicitly, the aim of CIS is to estimate the impulsive noise based on the principle of CS.**

10 successive samples are impaired by the above-mentioned 0.1 μs impulsive noise burst. Naturally, the long impulsive bursts of PLC may inflict bursts of errors. As a result, the system's performance may be severely degraded, especially in high data-rate transmissions relying on short symbol durations.

Orthogonal frequency-division multiplexing (OFDM), which is the predominant transmission technique of wireless communications at the time writing [11], [12], has also been adopted by the PLC standards, including IEEE P1901 [13], ITU-T G.hn [14] and HomePlug AV2 [15]. A frequency-selective fading channel can be converted into a number of parallel flat-fading subchannels with the aid of the OFDM, thereby, considerably reducing the receiver's complexity as a benefit of using single-tap frequency-domain equalization [11]. Cyclic prefix (CP)-based OFDM is employed to avoid the inter-OFDM-symbol interference [11]. Although the conventional OFDM signalling is capable of mitigating the mutipath effects of PLC, it experiences a performance loss in the presence of impulsive noise. In more detail, the discrete Fourier transform (DFT) spreads the effect of impulsive noise across all the subcarriers. When the duration of an impulsive burst is significantly shorter than the OFDM symbol duration, the associated spreading effect becomes beneficial, since all subcarriers are only marginally contaminated. Unfortunately, as mentioned above, the duration of impulsive noise in PLC may become substantially longer than the OFDM symbol duration, which significantly degrades the system performance, especially, when the power of impulsive noise is high. Therefore, conventional OFDM signalling is incapable of mitigating the impulsive noise in PLC.

As illustrated in the yellow part of Fig. 1, several methods have been proposed in the literature in order to mitigate the effect of impulsive noise imposed on OFDM systems communicating over PLC channels, such as nonlinear filtering [16]–[18], channel coding [19], [20], as well as both parametric and non-parametric estimation techniques [21], [22]. On the other hand, as shown by the blue part of Fig. 1, compressed sensing (CS), as an emerging theory, has attracted considerable research-attention, as exemplified by the elegant algorithms [23]–[28] of Fig. 1. CS has been proposed to tackle the issues of recovery of vectors in high dimensions from vectors in low dimensions, as detailed in [29]. Recently, CS has been invoked for solving numerous problems in communications systems, such as channel estimation [30], narrowband interference mitigation [31], spectrum sensing [32] and so on. Training-based impulsive noise estimation relying on CS also constitutes an attractive method, since it has several distinct advantages for OFDM systems communicating over PLC channels. Firstly, in practical PLCs, the high-attenuation frequency sub-bands of an OFDM symbol may be disabled for data transmissions [13], [15]. Hence, some of these deactivated tones can be used as training symbols for supporting training-based impulsive noise estimation. Secondly, it is possible to disperse the prolonged impulsive burst affecting numerous time-domain (TD) samples by simply using an interleaver.

In this way, the asynchronous impulsive noise can be estimated at a low complexity with the aid of CS. Finally, since the power of asynchronous impulsive noise is usually much higher than that of the background noise in BB-PLC, accurate impulsive noise estimation is attainable by using CS. The idea of applying CS to mitigate the impulse noise in OFDM systems was originally proposed in [33], where the impulse noise estimation was formulated as an ℓ_1-minimization problem. Later in [34], the mixed ℓ_2/ℓ_1-minimization has been employed for impulse noise estimation, where the impulsive noise was assumed to appear in form of sparse blocks. It should be noted that in [33] and [34] the duration of impulse noise was assumed to be much lower than that of an OFDM symbol, which is however, not the norm in PLCs. Furthermore, although the ℓ_1-minimization considered in [33] and the mixed ℓ_2/ℓ_1-minimization of [34] can be solved within polynomial rather than exponential time, the corresponding computational cost still remains excessive. It is important to emphasize that for both schemes substantial computational resources are required for estimating relatively insignificant impulsive noise, whose instantaneous power is lower than the modulation-dependent detection threshold.

Against the above background, in this paper, we propose a novel compressed impairment sensing (CIS)-assisted interleaving-double-FFT (IDFFT) based modulation scheme, which is capable of simultaneously mitigating both the multipath effects and the impulsive noise impairments in PLCs. It should be noted that similar to interleaved frequency division multiple access (IFDMA) [35], the proposed IDFFT system can be viewed as a special case of the DFT precoded OFDMA with interleaved subcarrier allocation. However, since the IDFFT system is specifically designed for CIS-assisted impulsive noise mitigation, the design objectives of IDFFT and IFDMA are different. The general philosophy of our proposed CIS-assisted IDFFT aided system transpires from Fig. 1. In the CIS-assisted IDFFT modulation systems, the transmitter carries out both an FFT and an IFFT operation, which are connected with a two-dimensional (2D) interleaver. Correspondingly, the receiver employs a frequency-domain (FD) equalizer and a CIS-assisted detector. The data symbols in our CIS-assisted IDFFT system are transmitted in the TD, while a FD equalizer is employed in order to achieve the maximum attainable multipath diversity gain [36]. In this paper, a 2D interleaver is conceived for dispersing the FD error-bursts, so that each transmission data block is only impaired by a few impulsive noise samples. In this way, the spreading effect of the FFT transforming the FD signal to the TD has a positive influence on the detection performance in the TD. Apart from this type of impulsive noise mitigation, we additionally propose a CIS-assisted algorithm for the estimation and cancellation of the impulsive noise. In this paper, the performance of our CIS-assisted IDFFT aided system is investigated with the aid of simulations. We demonstrate that our CIS-assisted IDFFT aided system outperforms conventional OFDM in the PLC environments experiencing both multipath propagation and asynchronous impulsive noise.

The rest of the paper is organized as follows. In Section II, the system model is detailed, where both the PLC channel and noise model are also described. The design of the 2D interleaver is considered in Section III. Then, our impulsive noise estimation and cancellation, as well as our proposed CIS-assisted signal detection algorithm are described in Section IV. In Section V, our simulation results are studied. Finally, we offer our conclusions in Section VI.

II. SYSTEM MODEL

A. PRELIMINARIES

For two disjoint index sets $\mathcal{I}_i$ and $\mathcal{I}_j$, we can readily show that $\boldsymbol{\Theta}_i^T\boldsymbol{\Theta}_i = \boldsymbol{I}_{M_i}$ and $\boldsymbol{\Theta}_i^T\boldsymbol{\Theta}_j = \mathbf{0}_{M_i\times M_j}$. Moreover, for a diagonal matrix $\boldsymbol{A}$ of size $M \times M$, we can also show that $\boldsymbol{\Theta}_i^T\boldsymbol{A}\boldsymbol{\Theta}_j = \mathbf{0}_{M_i\times M_j}$. For a matrix $\boldsymbol{A}$ of size $(M \times M)$, the submatrix of $\boldsymbol{A}$, whose columns (or rows) are extracted from $\boldsymbol{A}$ according to an index set $\mathcal{I}_i$, is denoted by $\boldsymbol{A}_i$ (or $\boldsymbol{A}_i^T$). We can show that $\boldsymbol{A}_i^T = \boldsymbol{\Theta}_i^T\boldsymbol{A}$ and $\boldsymbol{A}_i = \boldsymbol{A}\boldsymbol{\Theta}_i$.

B. TRANSMITTER

The proposed IDFFT aided transmitter is illustrated in Fig. 2. The data bits are first mapped into L_M blocks, each of which contains M_d data symbols, according to Q-ary QAM scheme having the alphabet $\mathcal{A}$. Let the L_M blocks of data symbols be expressed in a matrix form as $\boldsymbol{X}_\mathrm{d} = [\boldsymbol{x}_\mathrm{d}(0), \boldsymbol{x}_\mathrm{d}(1), \ldots, \boldsymbol{x}_\mathrm{d}(L_M-1)]$, where $\boldsymbol{x}_\mathrm{d}(l) \in \mathcal{A}^{M_\mathrm{d}\times 1}$ denotes the lth block of data symbols. Furthermore, we assume that $\mathbb{E}[|x_\mathrm{d}(m,l)|^2] = 1$, $\forall m, l$. In our IDFFT aided PLC systems, a total of M_p pilot symbols used for CIS are inserted into each of the blocks of data symbols. Since the impulsive noise is additive, zero-valued pilots are employed in order to save transmission power. Thus, after inserting the pilots, each data block contains $M = M_\mathrm{d} + M_\mathrm{p}$ symbols. Let the positions of pilots in a data block form an index set $\mathcal{I}_\mathrm{p}$, which is assumed to be the same for all blocks. Then, after inserting zero-valued pilots into $\boldsymbol{x}_\mathrm{d}$, the L_M blocks of data symbols $\boldsymbol{X}_\mathrm{T} = [\boldsymbol{x}_\mathrm{T}(0), \boldsymbol{x}_\mathrm{T}(1), \ldots, \boldsymbol{x}_\mathrm{T}(L_M-1)]$ can be expressed as

$$\boldsymbol{X}_\mathrm{T} = \boldsymbol{\Theta}_\mathrm{d}\boldsymbol{X}_\mathrm{d}, \tag{1}$$

where $\boldsymbol{\Theta}_\mathrm{d}$ is a mapping matrix based on the index set $\mathcal{I}_\mathrm{d} = \{0, 1, \ldots, M-1\}\backslash\mathcal{I}_\mathrm{p}$.

As shown in Fig. 2, the TD symbols $\boldsymbol{X}_\mathrm{T}$ are entered into the M-point FFT scheme block-by-block, yielding L_M blocks of FD symbols, which are expressed as

$$\begin{aligned}\boldsymbol{X}_\mathrm{F} &= [\boldsymbol{x}_\mathrm{F}(0), \boldsymbol{x}_\mathrm{F}(1), \ldots, \boldsymbol{x}_\mathrm{F}(L_M-1)] \\ &= \boldsymbol{\mathcal{F}}_M\boldsymbol{X}_\mathrm{T} = \boldsymbol{\mathcal{F}}_M\boldsymbol{\Theta}_\mathrm{d}\boldsymbol{X}_\mathrm{d},\end{aligned} \tag{2}$$

where $\boldsymbol{x}_\mathrm{F}(l) \in \mathbb{C}^{M\times 1}$ denotes the lth block of FD symbols, where it can be shown that we have $\mathbb{E}[\|\boldsymbol{x}_\mathrm{F}(l)\|^2] = M_\mathrm{d}/M, \forall l$. Next, as shown in Fig. 2, the FD symbols in $\boldsymbol{X}_\mathrm{F}$ are interleaved by the interleaver Π, yielding a new $(M \times L_M)$-element data matrix denoted as $\boldsymbol{S}_\mathrm{F} = [\boldsymbol{s}_\mathrm{F}(0), \boldsymbol{s}_\mathrm{F}(1), \ldots, \boldsymbol{s}_\mathrm{F}(L_M-1)]$,

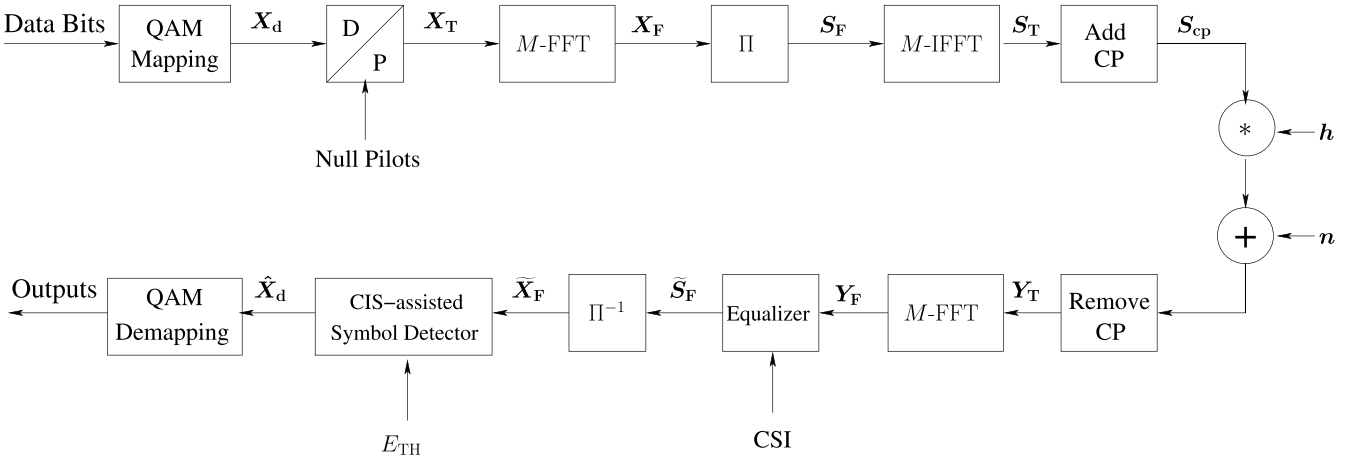

FIGURE 2. **Illustration of the CIS-assisted IDFFT system.**

where $\boldsymbol{s}_{\mathrm{F}}(l) \in \mathbb{C}^{M\times 1}, \forall l$. Note that the interleaver Π disperses the impulsive bursts encountered in both the FD and TD. Following the interleaving, an M-point IFFT is carried out block-by-block as shown in Fig. 2, yielding L_M blocks of TD symbols $\boldsymbol{S}_{\mathrm{T}} = [\boldsymbol{s}_{\mathrm{T}}(0), \boldsymbol{s}_{\mathrm{T}}(1), \ldots, \boldsymbol{s}_{\mathrm{T}}(L_M - 1)]$, which can be expressed as

$$\boldsymbol{S}_{\mathrm{T}} = \boldsymbol{\mathcal{F}}_M^H \boldsymbol{S}_{\mathrm{F}}. \tag{3}$$

Furthermore, in order to avoid ISI, a CP of length L_{cp} is inserted before each block of $\boldsymbol{S}_{\mathrm{T}}$, resulting in

$$\boldsymbol{S}_{\mathrm{cp}} = \boldsymbol{\Theta}_{\mathrm{CP}} \boldsymbol{S}_{\mathrm{T}}, \tag{4}$$

where $\boldsymbol{\Theta}_{\mathrm{CP}} = [\boldsymbol{\Theta}_{\mathrm{cp}}, \boldsymbol{I}_M]^T$ and $\boldsymbol{\Theta}_{\mathrm{cp}}$ is a mapping matrix formed by the last L_{cp} columns of an identity matrix $\boldsymbol{I}_M$. Finally, follows transmitter filtering, the symbols are sent block-by-block through the PLC channels imposing impulsive noise.

C. CHANNEL MODELLING

In this paper, we focus our attention on the PLC channels in the 1.8-100 MHz frequency range, which is the frequency band of interest for the current and next generation PLC systems. Due to the frequent connection and disconnection of various types of loads, as well as the presence of cable branches, indoor PLC channels exhibit a time-variant frequency-selective channel transfer function (CTF). Let $h_{\mathrm{F}}(f, t)$ denote the CTF between a given transmitter and its corresponding receive port in the power line at time t and frequency f. As shown in [2] and [5], the time variations of the PLC channels can be classified into two types, which are the short-term variation and long-term variation. In this paper, our focus is on the short-term variation of the PLC channels, which is dependent on the mains frequency and it is usually about hundreds of microseconds, hence we can assume that the PLC channels are time-invariant during L_H blocks of transmitted symbols. Then, when the signals of (4) are transmitted over the PLC channels and the received signals are sampled at an interval of Δt, the discrete-time baseband equivalent FD Channel Transfer Factor (FDCHTF) of the mth subchannel can be expressed as

$$h_{\mathrm{F}}(m) \triangleq h_{\mathrm{F}}\left(f = \frac{m}{T_s}, t = lT_s\right), \quad l = 0, 1, \ldots, L_M - 1, \tag{5}$$

where $T_s = M\Delta t$ denotes the symbol duration of an OFDM symbol. According to [6], the magnitude of the FDCHTF obeys the log-normal distribution expressed as $|h_{\mathrm{F}}(m)| \sim \text{Log-}\mathcal{N}[\Omega_H(m), \sigma_H^2(m)]$, where the mean $\Omega_H(m)$ and the variance $\sigma_H^2(m)$ are both dependent on the frequency of the mth subchannel. The phase of $h_{\mathrm{F}}(m)$ can be assumed to be uniformly distributed in $(-\pi, \pi), \forall m$.

D. NOISE MODELLING

We assume that the PLC channels encounter both background noise and asynchronous impulsive noise. The effects of narrowband interference are not considered in this treatise. This is because the narrowband interference usually appears in some particular sub-bands, thereby it can be readily eliminated by deactivating these sub-bands, as shown in [13], [15]. Hence, we focus our attention on mitigating the deleterious effects of both background noise and asynchronous impulsive noise. Whilst the background noise is present continuously, the asynchronous impulsive noise is sporadic. In detail, in the TD, the impulsive noise is characterized by three parameters [7]: its duration time t_1, inter-arrival time t_0 and its power. Naturally, during the inter-arrival time t_0, there is only background noise, while during the time t_1, both background noise and asynchronous impulsive noise are encountered. Explicitly, the measurement results of [7] have shown that both the duration and the inter-arrival time of asynchronous impulsive noise obeys an exponential distribution, i.e., $t_i \sim \mathrm{Exp}(\Omega_i)$ for $i = 0, 1$, where Ω_0 and Ω_1 are the average inter-arrival time and the average durations, respectively. Furthermore, let us define the ratio between the average duration of impulsive noise and the average inter-arrival time as $\Lambda_{\mathrm{T}} = \Omega_1/\Omega_0$. Let us denote the sampled background noise at the receiver by $\boldsymbol{n}_0$, which is complex

Gaussian distributed with zero mean and a variance of σ_0^2, i.e., $\boldsymbol{n}_0 \sim \mathcal{CN}(0, \sigma_0^2)$. Since the impulsive noise occurs with a random inter-arrival time t_0 and exists within a random duration t_1, we let $L_0 = [t_0/\Delta t]$ and $L_1 = [t_1/\Delta t]$, where $[x]$ represents an integer near x. Then, the sampled impulsive noise $\boldsymbol{n}_1$ of L_1–length can be modelled as a complex-valued Gaussian vector of zero mean and a variance of σ_1^2, i.e., $\boldsymbol{n}_1 \sim \mathcal{CN}(0, \sigma_1^2)$. Furthermore, the ratio between the impulsive noise power and background noise power is expressed as $\Lambda_{\mathrm{P}} = \sigma_1^2/\sigma_0^2$.

Let the mth sample of the lth symbol block be corrupted by the noise samples $n_{\mathrm{T}}(m, l)$. Based on the above-mentioned characterization of PLC channel noise, $n_{\mathrm{T}}(m, l)$ can be expressed as

$$n_{\mathrm{T}}(m, l) = n_0(m, l) + c_{n_1}(m, l) n_1(m, l), \tag{6}$$

where $n_q(m, l) \sim \mathcal{CN}(0, \sigma_q^2)$ with $q \in \{0, 1\}$, while $c_{n_1}(m, l) \in \{0, 1\}$ is defined as the occurrence indicator of impulsive noise, which is dependent on both the duration time t_1 and the inter-arrival time t_0.

E. RECEIVED FD SIGNALS

Let us assume that perfect time synchronization has been achieved by the receiver. Moreover, we assume that the length of the CP is higher than the PLC channel's maximum delay spread, while the bandwidth of each subchannel is significantly lower than the PLC channel's coherence bandwidth. Then, as shown in Fig. 2, after removing the CP, the received baseband equivalent observations of the L_M blocks of data are given by $\boldsymbol{Y}_{\mathrm{T}} = [\boldsymbol{y}_{\mathrm{T}}(0), \boldsymbol{y}_{\mathrm{T}}(1), \ldots, \boldsymbol{y}_{\mathrm{T}}(L_M - 1)]$, which can be formulated as

$$\boldsymbol{Y}_{\mathrm{T}} = \widetilde{\boldsymbol{H}} \boldsymbol{S}_{\mathrm{T}} + \boldsymbol{N}_{\mathrm{T}}, \tag{7}$$

where $\widetilde{\boldsymbol{H}}$ is an $(M \times M)$ circulant matrix, which can be diagonalized by the M-point DFT matrix, given by $\widetilde{\boldsymbol{H}} = \boldsymbol{\mathcal{F}}_M^H \boldsymbol{H} \boldsymbol{\mathcal{F}}_M$, where $\boldsymbol{H} = \mathrm{diag}\{h_{\mathrm{F}}(0), h_{\mathrm{F}}(1), \ldots, h_{\mathrm{F}}(M-1)\}$ and $h_{\mathrm{F}}(m)$ represents the channel gain of the mth subchannel, which can be generated by the statistical modelling described in Section II-C. In (7), the noise samples in $\boldsymbol{N}_{\mathrm{T}} \in \mathbb{C}^{M \times L_M}$ contain the background noise and possibly impulsive noise, which is shown in (6).

As seen in Fig. 2, upon carrying out the FFT of $\boldsymbol{Y}_{\mathrm{T}}$, we obtain

$$\begin{aligned} \boldsymbol{Y}_{\mathrm{F}} &= \boldsymbol{\mathcal{F}}_M \boldsymbol{Y}_{\mathrm{T}} \\ &= \boldsymbol{\mathcal{F}}_M \boldsymbol{\mathcal{F}}_M^H \boldsymbol{H} \boldsymbol{\mathcal{F}}_M \boldsymbol{S}_{\mathrm{T}} + \boldsymbol{\mathcal{F}}_M \boldsymbol{N}_{\mathrm{T}} \\ &= \boldsymbol{H} \boldsymbol{\mathcal{F}}_M \boldsymbol{\mathcal{F}}_M^H \boldsymbol{S}_{\mathrm{F}} + \boldsymbol{N}_{\mathrm{F}} \\ &= \boldsymbol{H} \boldsymbol{S}_{\mathrm{F}} + \boldsymbol{N}_{\mathrm{F}}, \end{aligned} \tag{8}$$

where $\boldsymbol{N}_{\mathrm{F}} = \boldsymbol{\mathcal{F}}_M \boldsymbol{N}_{\mathrm{T}}$ denotes the FD noise. Note that, when a block of symbols is corrupted by impulsive noise in the TD, depending on the duration of impulsive noise, the FFT operation may have either a positive or a negative effect on the attainable detection performance, which can be explained as follows. Firstly, let the lth block be corrupted by an $L_1(l)$-length impulsive noise in the TD, where $L_1(l) \in \{0, 1, \ldots, M\}$. Then, we can show that $\boldsymbol{N}_{\mathrm{F}}(l) \sim \mathcal{CN}[0, \sigma_{\mathrm{n}}^2(l)]$, where the variance $\sigma_{\mathrm{n}}^2(l)$ can be expressed as

$$\begin{aligned} \sigma_{\mathrm{n}}^2(l) &= \sigma_0^2 + \frac{L_1(l)}{M} \sigma_1^2 \\ &= \left[1 + \frac{L_1(l)}{M} \Lambda_{\mathrm{P}}\right] \sigma_0^2. \end{aligned} \tag{9}$$

Observe from (9) that if $L_1(l)$ is large enough, all the subchannels in the FD may be impaired by high-power noise. As a result, the detection performance may be severely degraded. In order to mitigate the effect of impulsive noise, in this paper, both FD equalization and TD CIS are employed with the aid of the interleaver Π.

As shown in Fig. 2, before de-interleaving, the FD symbols in $\boldsymbol{Y}_{\mathrm{F}}$ are first equalized. Let us define the power ratio between the signal and background noise as $\gamma_{\mathrm{s},0} = \mathbb{E}[\|\boldsymbol{s}\|_2^2]/\mathbb{E}[\|\boldsymbol{n}_0\|_2^2] = 1/\sigma_0^2$, which is assumed to be known as *a priori* information at the receiver. Moreover, we stipulate the idealized simplifying assumption that perfect channel estimation is achieved at the receiver. Then, we use an minimum mean square error (MMSE) equalizer, whose weight matrix is given by $\boldsymbol{W} = \left[\boldsymbol{H}^H \boldsymbol{H} + (1/\gamma_{\mathrm{s},0}) \boldsymbol{I}_M\right]^{-1} \boldsymbol{H}^H$. Hence, after MMSE equalization, the lth block of equalised symbols $\widetilde{\boldsymbol{s}}_{\mathrm{F}}(l)$ can be expressed as

$$\begin{aligned} \widetilde{\boldsymbol{s}}_{\mathrm{F}}(l) &= \boldsymbol{W} \boldsymbol{y}_{\mathrm{F}}(l) \\ &= \boldsymbol{W} \boldsymbol{H} \boldsymbol{s}_{\mathrm{F}}(l) + \boldsymbol{W} \boldsymbol{n}_{\mathrm{F}}(l) \\ &= \boldsymbol{R} \boldsymbol{s}_{\mathrm{F}}(l) + \widetilde{\boldsymbol{n}}_{\mathrm{F}}(l), \quad l = 0, 1, \ldots, L_M - 1, \end{aligned} \tag{10}$$

where $\boldsymbol{R} = \boldsymbol{W}\boldsymbol{H}$ is a diagonal matrix, whose mth diagonal element is given by

$$R(m) = \frac{|h_{\mathrm{F}}(m)|^2}{|h_{\mathrm{F}}(m)|^2 + \frac{1}{\gamma_{\mathrm{s},0}}}, \quad m = 0, 1, \ldots, M-1, \tag{11}$$

while $\widetilde{\boldsymbol{n}}_{\mathrm{F}}(l) = \boldsymbol{W} \boldsymbol{n}_{\mathrm{F}}(l)$ denotes the filtered noise. Eq. (11) shows that the MMSE equalizer is capable of mitigating the background noise, but at the cost of some loss in signal power. Furthermore, we can readily show that the signal to interference plus noise power ratio (SINR) achieved for the mth subchannel of the lth block is

$$\mathrm{SINR}(m, l) = \frac{|h_{\mathrm{F}}(m)|^2}{\sigma_{\mathrm{n}}^2(l)}. \tag{12}$$

As shown in Fig. 2, after FD equalization, the L_M blocks of symbols $\widetilde{\boldsymbol{S}}_{\mathrm{F}} = [\widetilde{\boldsymbol{s}}_{\mathrm{F}}(0), \widetilde{\boldsymbol{s}}_{\mathrm{F}}(1), \ldots, \widetilde{\boldsymbol{s}}_{\mathrm{F}}(L_M - 1)]$ are input to the de-interleaver Π^{-1}. In the next section, we consider the design of the interleaver Π.

III. DESIGN OF THE 2D INTERLEAVER

The measurements results of [7], [37], and [38] show that in indoor PLCs, the average duration of impulsive noise bursts is much longer than the symbol duration used in the existed standards [13]–[15]. Thus, when there is an impulsive burst, multiple successive symbols may be corrupted. In order to

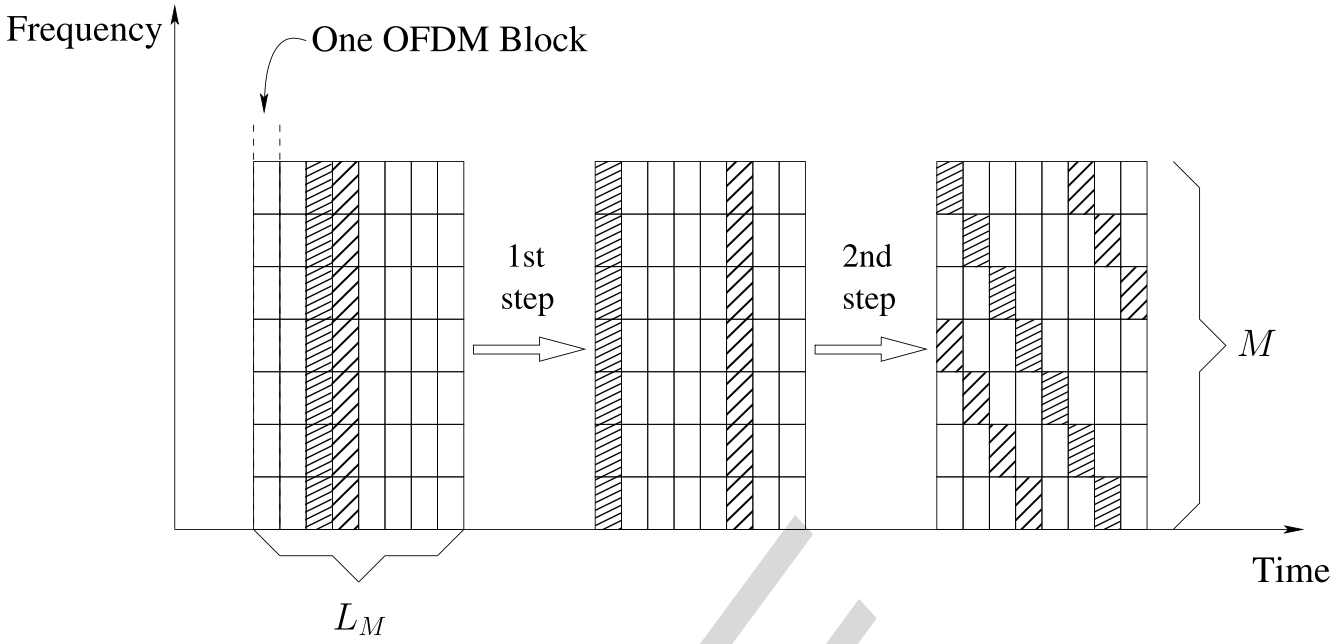

FIGURE 3. Illustration of interleaving process of the 2D Interleaver Π.

distribute the effect of bursty impulsive noise, a 2D interleaver Π is employed. Let us first consider our design criteria related to the 2D interleaver. As shown in (12), when the mth subchannel experiences a high attenuation or the noise variance $\sigma_{\mathrm{n}}^2(l)$ is high, the SINR becomes low. Since the FDCHTFs are assumed to be constant over L_M blocks, the interleaver should be designed to guarantee that the data symbols transmitted by the same subchannel are not permuted into the same data block after de-interleaving. Similarly, when there is an impulsive burst, its effect should be evenly distributed to as many blocks as possible after de-interleaving. In this way, with the aid of the spreading effect of the IFFT to be carried out in the receiver, each block of the TD data symbols will be impaired by the impulsive noise having a relatively low power.

Based on the above analysis, a 2D interleaver is designed, whose operations are illustrated in Fig 3. In this treatise, we focus our attention on investigating the beneficial effects of interleaving on mitigating impulsive noise. Hence, the length of the 2D interleaver Π in TD has to be lower than the coherence time of PLC channels, i.e. we have $L_\Pi = L_M M < L_H M$, where L_H was defined in Section II-D. Thus, the multipath diversity gain attained by interleaving is not considered in this paper. Explicitly, during the transmission of L_M blocks of TD symbols denoted as $\boldsymbol{X}_{\mathrm{F}}$, the blocks' order is first interleaved by the S-random interleaver having a minimum distance[1] of $S = \sqrt{a_\Pi L_M}$ [39]–[41], where $a_\Pi > 0$ is a constant. Note that, the S-random interleaver is employed in the first step as a benefit of its resilience against bursty impulsive noise [42]. Then, as shown in Fig. 3, for the mth row of $\boldsymbol{X}_{\mathrm{F}}$, the element in the lth column is circularly shifted to the l^Πth column, where we have $l^\Pi = l + m \mod L_M$. In this way, even if all the M FD samples of a block experience impulsive noise, after the de-interleaving stage of Fig. 3, they will become distributed across M different blocks, each of which contains only a single impulsive noise sample from the impaired original block. Additionally, the interleaving scheme guarantees that the data symbols conveyed by the same subchannel of different blocks will not be permuted to the same block.

As shown in Section II-D, the duration t_1 of asynchronous impulsive noise can be modelled by the exponential distribution having a mean of Ω_1. When L_M OFDM blocks are corrupted by asynchronous impulsive noise with a duration of t_1, the dispersion capability of the above-mentioned 2D interleaver can be measured in term of the complementary cumulative distribution function (CCDF) of t_1, which can be expressed as

$$P\left(t_1 > \frac{L_\Pi}{\varepsilon_\Pi}\Delta t\right) = P\left(t_1 > \frac{L_M}{\varepsilon_\Pi} M\Delta t\right) = \exp\left(-\frac{L_M \Delta t}{\varepsilon_\Pi \Omega_1} M\right), \quad (13)$$

where ε_Π is the spreading factor of the 2D interleaver Π, as defined in [40]. It can be readily shown that the spreading factor of the above-mentioned 2D interleaver Π is given by $\varepsilon_\Pi = \min\{M+1, S+1\} = \min\{M+1, \sqrt{a_\Pi L_M}+1\}$. Clearly, the smaller the probability formulated in (13), the better the dispersion capability of the 2D interleaver Π. Hence, as it will be shown in Section V-B, the value of L_M can be

[1] As defined in [39], the S-random interleaver is a pseudo-random interleaver with the restriction that any two indices within a distance of S cannot be permuted to indices within a distance of S, where S is known as the minimum distance of the S-random interleaver.

carefully chosen so that the probability formulated in (13) is sufficiently low for meeting a specific design criterion.

A. CLASSIFICATION OF DE-INTERLEAVED NOISE SAMPLES

Let the received FD symbols in $\widetilde{\boldsymbol{S}}_{\mathrm{F}}$ be input into the de-interleaver Π^{-1}, yielding an $(M \times L_M)$ symbol matrix expressed as $\widetilde{\boldsymbol{X}}_{\mathrm{F}} = [\widetilde{\boldsymbol{x}}_{\mathrm{F}}(0), \widetilde{\boldsymbol{x}}_{\mathrm{F}}(1), \ldots, \widetilde{\boldsymbol{x}}_{\mathrm{F}}(L_M - 1)]$, where the lth block of de-interleaved symbols $\widetilde{\boldsymbol{x}}_{\mathrm{F}}(l) \in \mathbb{C}^{M\times 1}$ can be expressed as

$$\widetilde{\boldsymbol{x}}_{\mathrm{F}}(l) = \boldsymbol{R}\boldsymbol{x}_{\mathrm{F}}(l) + \widetilde{\boldsymbol{n}}'_{\mathrm{F}}(l), \tag{14}$$

with $\widetilde{\boldsymbol{n}}'_{\mathrm{F}}(l)$ being the de-interleaved version of $\widetilde{\boldsymbol{n}}_{\mathrm{F}}(l)$ in (10). Here, due to the specific design of the 2D interleaver Π, the diagonal matrix $\boldsymbol{R}$ shown in (14) remains the same after de-interleaving. In practice, the transmitted signal power should be sufficiently high in order to guarantee the required quality-of-service (QoS). Thus, in this subsection, we only consider a scenario, when the system's performance is dominated by the impulsive noise. In this case, we can rewrite (14) as

$$\widetilde{\boldsymbol{x}}_{\mathrm{F}}(l) = \boldsymbol{x}_{\mathrm{F}}(l) + \boldsymbol{g}_{\mathrm{F}}(l) + \widetilde{\boldsymbol{n}}'_{\mathrm{F}}(l), \tag{15}$$

where $\boldsymbol{g}_{\mathrm{F}}(l) = [\boldsymbol{R} - \boldsymbol{I}_M]\boldsymbol{x}_{\mathrm{F}}(l)$ is the residual interference. In (15), the FD symbols in $\boldsymbol{x}_{\mathrm{F}}(l)$ exhibit a high peak-to-average power ratio (PAPR) due to the FFT operation of the transmitter. This property makes it hard to identify whether a sample experiences impulsive noise. In our proposed IDFFT aided system, when an equal power allocation policy is employed, according to the studies in [43], the CCDF of the corresponding PAPR can be expressed as

$$P(\mathrm{PAPR} > x) \approx 1 - \exp\left(-e^{-x}\sqrt{\frac{M_{\mathrm{p}}M_{\mathrm{d}}^3\pi x}{3M^2}}\right). \tag{16}$$

Let us define a threshold E_{TH}, which is used for identifying whether a sample experiences impulsive noise. In order to enhance the accuracy of the identification, with the aid of (16), the value of the threshold E_{TH} may be chosen by satisfying

$$E_{\mathrm{TH}} \quad \text{s.t.} \quad P\left(\mathrm{PAPR} > E_{\mathrm{TH}}\right) = \varepsilon_{\mathrm{small}}, \tag{17}$$

where s.t. is short for "subject to", while $\varepsilon_{\mathrm{small}}$ denotes a small probability specified by the design.

Then, by comparing the FD symbols in $\widetilde{\boldsymbol{x}}_{\mathrm{F}}(l)$ against the threshold E_{TH}, a binary indicator sequence $\boldsymbol{c}_{\mathrm{detect}}(l)$ can be obtained, where we have

$$c_{\mathrm{detect}}(m, l) = \begin{cases} 1, & \text{if } |\widetilde{x}_{\mathrm{F}}(m, l)|^2 > E_{\mathrm{TH}} \\ 0, & \text{otherwise.} \end{cases} \tag{18}$$

Furthermore, let us define $\mathcal{I}_1(l) = Supp\{\boldsymbol{c}_{\mathrm{detect}}(l)\}$ and $\mathcal{I}_0(l) = \{0, 1, \ldots, M-1\}\backslash\mathcal{I}_1(l)$. Then, $\widetilde{\boldsymbol{n}}'_{\mathrm{F}}(l)$ seen in (15) can be written as

$$\widetilde{\boldsymbol{n}}'_{\mathrm{F}}(l) = \boldsymbol{n}_0(l) + \boldsymbol{n}_1(l), \tag{19}$$

where, for $q \in \{0, 1\}$, we have $n_q(m, l) = \widetilde{n}'_{\mathrm{F}}(m, l)$ if $m \in \mathcal{I}_q(l)$, otherwise, $n_q(m, l) = 0$. Substituting (19) into (15), we arrive at

$$\widetilde{\boldsymbol{x}}_{\mathrm{F}}(l) = \boldsymbol{x}_{\mathrm{F}}(l) + \boldsymbol{g}_{\mathrm{F}}(l) + \boldsymbol{n}_0(l) + \boldsymbol{n}_1(l). \tag{20}$$

Based on the above analysis, the noise samples classified into $\mathcal{I}_1(l)$ are deemed to be contributed by impulsive noise with a high probability. Our proposed interleaving scheme is capable of uniformly distributing the impulsive bursts, when the value of ε_Π shown in (13) is chosen to be high enough. When this is the case, we can readily show that

$$k(l) = \|\boldsymbol{n}_1(l)\|_0 < \left\lceil \frac{L_\Pi}{\varepsilon_\Pi L_M} \right\rceil = \left\lceil \frac{M}{\varepsilon_\Pi} \right\rceil \ll M, \tag{21}$$

implying that the vector $\boldsymbol{n}_1(l)$ is a sparse vector with a sparsity level given by $k(l) = \|\boldsymbol{n}_1(l)\|_0$.

Finally, as shown in Fig. 2, the de-interleaved FD symbols in $\widetilde{\boldsymbol{x}}_{\mathrm{F}}(l)$ are input to a CIS-assisted symbol detector, which is detailed in the next section.

IV. CIS-ASSISTED SYMBOL DETECTOR

Typically, the optimum detector based on the maximum *a posteriori* (MAP) design rule is invoked for solving the following optimization problem

$$x_{\mathrm{d}}^{\mathrm{MAP}}(m, l) = \arg\max_{x_{\mathrm{d}}(m,l)\in\mathcal{A}} \left\{P\left(x_{\mathrm{d}}(m, l)|\widetilde{\boldsymbol{x}}_{\mathrm{F}}(l)\right)\right\}, \tag{22}$$

where $P\left(x_{\mathrm{d}}(m, l)|\widetilde{\boldsymbol{x}}_{\mathrm{F}}(l)\right)$ is the *a posteriori* probability at the receiver's output. It should be noted that the symbol vector $\widetilde{\boldsymbol{x}}_{\mathrm{F}}(l)$ contains pilot symbols. As shown in Section II, the pilots are invoked for estimating the impulsive noise having a high instantaneous power, which are actually the non-zero elements in $\boldsymbol{n}_1(l)$, as shown in (20). Assuming that perfect estimation of $\boldsymbol{n}_1(l)$ can be achieved with the aid of the pilots, the corresponding noise-plus-interference power is reduced, i.e. the SINR formulated in (12) is increased. Thus, the detection performance of the MAP-receiver represented by (22) can be improved. Therefore, instead of solving (22) directly, in this section, we propose a CIS-assisted symbol detector for our IDFFT system. Firstly, we will show that the non-zero elements in $\boldsymbol{n}_1(l)$ can be readily estimated with the aid of the pilot symbols relying on the principle of CS. Then, in order to achieve accurate estimation, we introduce a search algorithm for designing the pilots. Finally, a CIS-assisted symbol detector is proposed for detecting the transmitted data symbols.

A. COMPRESSED IMPAIRMENT SENSING (CIS) FOR IMPULSIVE NOISE ESTIMATION

Since the zero-valued TD pilots have been used for impulsive noise estimation, the lth block of received pilot symbols can be expressed as

$$\begin{aligned} \boldsymbol{y}_{\mathrm{p}}(l) &= \boldsymbol{\Theta}_{\mathrm{p}}^T\boldsymbol{\mathcal{F}}_M^H\widetilde{\boldsymbol{x}}_{\mathrm{F}}(l) \\ &= \boldsymbol{\Theta}_{\mathrm{p}}^T\boldsymbol{\mathcal{F}}_M^H\boldsymbol{n}_1(l) + \boldsymbol{\Theta}_{\mathrm{p}}^T\boldsymbol{\mathcal{F}}_M^H\left[\boldsymbol{n}_0(l) + \boldsymbol{g}_{\mathrm{F}}(l)\right] \\ &= \boldsymbol{A}\boldsymbol{n}_1(l) + \boldsymbol{n}_{\mathrm{p}0}(l), \end{aligned} \tag{23}$$

where $\boldsymbol{A} = \boldsymbol{\Theta}_{\mathrm{p}}^{T}\boldsymbol{\mathcal{F}}_{M}^{H}$ is the measurement matrix for $\boldsymbol{n}_1(l)$, which has the size of $(M_{\mathrm{p}} \times M)$ and it is known to the detector, while $\boldsymbol{n}_{\mathrm{p0}}(l)$ denotes the TD residual interference plus noise. According to [44] and [45], when the SNR is relatively high or when M is large, the TD residual interference plus noise $\boldsymbol{n}_{\mathrm{p0}}(l)$ seen in (23) can be approximated by Gaussian noise.

According to our analysis in Section III, the noise vector $\boldsymbol{n}_1(l)$ is usually a sparse vector, as shown in (21), which again may be estimated using the principles of CS. Specifically, given the observation equation in the form of (23), the sparse vector $\boldsymbol{n}_1(l)$ can be recovered by solving an ℓ_0-minimization problem [46], [47], which is described as

$$\hat{\boldsymbol{n}}_1^{\ell_0}(l) = \underset{\boldsymbol{n}_1(l)\in\mathbb{C}^{M\times 1}}{\arg\min} \{\|\boldsymbol{n}_1(l)\|_0\}, \quad \text{s.t. } \boldsymbol{y}_{\mathrm{p}}(l) - \boldsymbol{A}\boldsymbol{n}_1(l) \in \mathcal{B}, \tag{24}$$

where $\mathcal{B}$ is a bounded set associated with the noise $\boldsymbol{n}_{\mathrm{p0}}(l)$. However, the ℓ_0-minimization problem shown in (24) has been proved to be NP-hard [48]. For this reason, in CS, typically the ℓ_1-minimization based solutions are employed, since they are tractable to solve. According to [29], under certain conditions, the ℓ_0-minimization problem shown of (24) is equivalent to solving the ℓ_1-minimization problem of

$$\hat{\boldsymbol{n}}_1^{\ell_1}(l) = \underset{\boldsymbol{n}_1(l)\in\mathbb{C}^{M\times 1}}{\arg\min} \{\|\boldsymbol{n}_1(l)\|_1\}, \quad \text{s.t. } \boldsymbol{y}_{\mathrm{p}}(l) - \boldsymbol{A}\boldsymbol{n}_1(l) \in \mathcal{B}. \tag{25}$$

Note that the ℓ_1-minimization problem is a well-known convex optimisation problem, which can be solved in polynomial time, for example, by the interior point method [49]. However, when the impulsive noise estimation technique of this paper is considered, the computational cost of solving the ℓ_1-minimization problem still remains excessive. Hence, algorithms imposing even lower computational cost are required, such as the family of greed algorithms [26], [27].

Regardless, whether the ℓ_1-minimization based algorithms or the greedy algorithms are employed, the estimation precision is dependent on the structure of the measurement matrix $\boldsymbol{A} = \boldsymbol{\Theta}_{\mathrm{p}}^{T}\boldsymbol{\mathcal{F}}_{M}^{H}$ of (23), which is in turn determined by the specific positions of the pilot symbols. Therefore, below we consider the pilot design conceived for our IDFFT aided systems.

B. PILOT DESIGN FOR IDFFT AIDED SYSTEMS

In CS, the mutual incoherence property (MIP)[2] [50] and the restricted isometry property (RIP)[3] [51] are related to the design of the measurement matrix, which are commonly used for estimation-accuracy analysis in CS. However, it is usually hard to verify whether a measurement matrix satisfies the RIP, since computing the restricted isometry constant has been proved to be NP-hard [52]. On the other hand, a measurement matrix is said to satisfy the MIP, if it has a small mutual coherence. Here, the mutual coherence of a measurement matrix is defined as the largest absolute correlation coefficient between any two columns of the matrix. Since the mutual coherence can be readily computed, the MIP is often applied in some practical applications of CS. Specifically, the measurement matrix $\boldsymbol{A}$ defined in (23) is actually a partial Fourier matrix, whose mutual coherence is given by [53]

$$\begin{aligned}\mu &= \max_{0\le l_1<l_2\le M-1} \frac{\left|(\boldsymbol{a}(l_1))^H\boldsymbol{a}(l_2)\right|}{\|\boldsymbol{a}(l_1)\|_2\|\boldsymbol{a}(l_2)\|_2} \\ &= \max_{0\le l_1<l_2\le M-1} \frac{1}{M_{\mathrm{p}}}\left|\sum_{i=0}^{M_{\mathrm{p}}-1}\exp\left\{j\frac{2\pi\mathcal{I}_{\mathrm{p}}(i)}{M}(l_1-l_2)\right\}\right| \\ &= \max_{1\le l\le M-1} \frac{1}{M_{\mathrm{p}}}\left|\sum_{i=0}^{M_{\mathrm{p}}-1}\exp\left\{j\frac{2\pi l}{M}\mathcal{I}_{\mathrm{p}}(i)\right\}\right|, \end{aligned} \tag{26}$$

where $\boldsymbol{a}(x)$ denotes the xth column of $\boldsymbol{A}$, while $l = (l_1 - l_2) \bmod M$. As shown in (26), the mutual coherence of matrix $\boldsymbol{A}$ depends on the corresponding index set $\mathcal{I}_{\mathrm{p}}$, giving the specific positions of the pilots. Let us define a binary sequence $\boldsymbol{c}_{\mathrm{p}} = [c_{\mathrm{p}}(0), c_{\mathrm{p}}(1), \ldots, c_{\mathrm{p}}(M-1)]^T$, where $c_{\mathrm{p}}(m) = 0$, $\forall m \notin \mathcal{I}_{\mathrm{p}}$, while $c_{\mathrm{p}}(\mathcal{I}_{\mathrm{p}}(i)) = 1$ for $i = 0, 1, \ldots, M_{\mathrm{p}}-1$. Then, (26) can be equivalently expressed as

$$\mu = \max_{1\le l\le M-1} \frac{1}{M_{\mathrm{p}}}\left|\sum_{m=0}^{M-1} c_{\mathrm{p}}(m)\exp\left\{j\frac{2\pi ml}{M}\right\}\right|. \tag{27}$$

It can be shown that the mutual coherence μ of matrix $\boldsymbol{A} \in \mathbb{C}^{M_{\mathrm{p}}\times M}$ is bounded by

$$\sqrt{\frac{M-M_{\mathrm{p}}}{M_{\mathrm{p}}(M-1)}} \le \mu \le 1, \tag{28}$$

where the lower bound at the left hand side is the well-known Welch bound [53]. If the mutual coherence μ achieves the Welch bound, we say that matrix $\boldsymbol{A}$ is a maximum-Welch-bound-equality (MWBE) codebook [54], which is also known as an equiangular tight frame (ETF) [55]. Hence, in order to achieve the minimum mutual coherence, or in other words to obtain the MWBE codebook for the partial Fourier matrix, the pilots' position indices $\mathcal{I}_{\mathrm{p}}$ or binary sequence $\boldsymbol{c}_{\mathrm{p}}$ can be designed by solving the following problem

$$\begin{aligned}\boldsymbol{c}_{\mathrm{p}}^{(opt)} &= \arg\min_{\boldsymbol{c}_{\mathrm{p}}}\left\{\max_{1\le l\le M-1}\frac{1}{M_{\mathrm{p}}}\left|\sum_{m=0}^{M-1}c_{\mathrm{p}}(m)\exp\left\{j\frac{2\pi ml}{M}\right\}\right|\right\} \\ &= \sqrt{\frac{M-M_{\mathrm{p}}}{M_{\mathrm{p}}(M-1)}}. \end{aligned} \tag{29}$$

In practice, the IDFT matrix $\boldsymbol{\mathcal{F}}_{M}^{H}$ is usually selected to satisfy $M = 2^{\alpha}$, in order to achieve high estimation-speed, low-power consumption, as well as low round-off error.

[2]The MIP is defined as the mutual coherence of a matrix is very small [50].

[3]As defined in [51], the RIP is defined as the kth restricted isometry constant δ_k of matrix $\boldsymbol{A}$ is the smallest number such that $(1-\delta_k)\|\boldsymbol{x}\|_2^2 \le \|\boldsymbol{A}\boldsymbol{x}\|_2^2 \le (1+\delta_k)\|\boldsymbol{x}\|_2^2$ is satisfied for any k-sparse vectors $\boldsymbol{x}$.

When this type of IDFT matrix is considered, there is a paucity of information concerning the MWBE codebook. Furthermore, there are no known analytical approaches for the construction of the MWBE codebook in the case of $M = 2^{\alpha}$. Consequently, the near-optimal codebooks have been proposed in the literature [56]–[59], aiming at finding the near-optimal binary sequences $\hat{\boldsymbol{c}}_{\mathrm{p}}$ by solving the optimization problem of

$$\hat{\boldsymbol{c}}_{\mathrm{p}} = \arg\min_{\boldsymbol{c}_{\mathrm{p}}} \left\{ \max_{1\le l\le M-1} \frac{1}{M_{\mathrm{p}}} \left| \sum_{m=0}^{M-1} c_{\mathrm{p}}(m) \exp\left\{ j\frac{2\pi ml}{M} \right\} \right| \right\}. \tag{30}$$

Specifically, in [56], the authors have shown that, when $\boldsymbol{c}_{\mathrm{p}}$ is a binary Golay sequence, it is possible to construct a codebook, whose mutual coherence is approximately $\sqrt{2}$ times higher than the Welch bound, provided that M is sufficiently high. However, this approach is not flexible, since the value of M_{p} is fixed. Another concern is that for the design of pilot symbols, the value of M_{p} suitable for binary Golay sequences is excessive for practical application. Therefore, often numerical search methods have been applied [57]–[59]. Specifically, the brute-force search [57], the modified Lloyd search algorithm [58], and a search method based on smooth sequential optimization relying on the Grassmannian manifold [59] have been considered. However, these search algorithms typically exhibit a high computational complexity. Based on the above observation, in this section, we propose a low-complexity search algorithm for the design of the measurement matrix $\boldsymbol{A}$, which determines the positions of the pilots.

Firstly, let us define $\check{\boldsymbol{c}}_{\mathrm{p}} = \boldsymbol{\mathcal{F}}^{H}_{M-1}\boldsymbol{c}_{\mathrm{p}}$, where $\boldsymbol{\mathcal{F}}^{H}_{M-1}$ is obtained by eliminating the zeroth row of $\boldsymbol{\mathcal{F}}^{H}_{M}$. Then, (30) can be rewritten as

$$\hat{\check{\boldsymbol{c}}}^{'}_{\mathrm{p}} = \arg\min_{\check{\boldsymbol{c}}_{\mathrm{p}}} \left\{ \max_{0\le l'\le M-2} \frac{\left|\check{c}_{\mathrm{p}}(l')\right|}{M_{\mathrm{p}}} \right\}, \tag{31}$$

where $\check{c}_{\mathrm{p}}(l')$ is the l'th element of $\check{\boldsymbol{c}}_{\mathrm{p}}$. Our search procedure is formulated in Algorithm 1.

To elaborate further on the above algorithm, the mutual coherence is calculated from (31), where only the single variable l' is required. Therefore, the complexity of calculating the mutual coherence is on the order of $\mathcal{O}(M)$. For a large M, the complexity of our algorithm is significantly lower than that of the conventional approaches [57], [58]. Moreover, as shown in line 8 of Algorithm 1, by taking advantage of the Fourier transform, the L_c number of candidates can be calculated simultaneously, instead of being calculated successively. Therefore, our algorithm constitutes an efficient search technique.

C. CIS-ASSISTED SIGNAL DETECTION

In Section IV-A, we have shown that it is possible to estimate the noise samples in $\boldsymbol{n}_1(l)$ based on the principles of CS with the aid of the proposed pilot design. Moreover, as shown in Section III-A, the indices of the non-zero elements

Algorithm 1 Find the Optimal Solution of (31)

Require: $M, M_{\mathrm{p}}, \boldsymbol{\mathcal{F}}^{H}_{M-1}$

1: **Initialization**: Set $\mathcal{I}_M = [0, 1, \ldots, M-1]$, $\hat{\mu} = 1$, the number of candidates to L_c, and $\hat{\boldsymbol{c}}_{\mathrm{p}} = \emptyset$;
2: **for** $t = 1$ to T **do**
3: Set $\boldsymbol{C}_{\mathrm{p}} = \boldsymbol{0}_{M\times L_c}$;
4: **for** $l = 1$ to L_c **do**
5: Randomly permute $\mathcal{I}_M$; then, collect the first M_{p} elements into $\mathcal{I}_{\mathrm{p}}(l)$;
6: The elements in the lth column of $\boldsymbol{C}_{\mathrm{p}}$ are updated by

$$C_{\mathrm{p}}(m, l_c) = \begin{cases} 1, & \text{if } m \in \mathcal{I}_{\mathrm{p}}(l_c) \\ 0, & \text{otherwise} \end{cases};$$

7: **end for**
8: Calculate $\check{\boldsymbol{C}}_{\mathrm{p}} = \frac{1}{M_{\mathrm{p}}}\boldsymbol{\mathcal{F}}^{H}_{M-1}\boldsymbol{C}_{\mathrm{p}}$;
9: Find the index $\hat{l}_c$ by solving ▷ (30)←(31)

$$\hat{l}_c = \arg\min_{l_c=1,2,\ldots,L_c} \left\{ \max_{0\le m\le M-2} \left|\check{C}_{\mathrm{p}}(m, l_c)\right| \right\};$$

10: Obtain $\check{\mu}(\hat{l}_c) = \max_{0\le m\le M-2} \left|\check{C}_{\mathrm{p}}(m, \hat{l}_c)\right|$; ▷ (31)
11: **if** $\check{\mu}(\hat{l}_c) < \hat{\mu}$ **then**
12: $\hat{\mu} = \check{\mu}(\hat{l}_c)$;
13: $\hat{\boldsymbol{c}}_{\mathrm{p}} = \boldsymbol{C}_{\mathrm{p}}(\hat{l}_c)$;
14: **end if**
15: **end for**
16: **return** $\hat{\mu}$ and $\hat{\boldsymbol{c}}_{\mathrm{p}}$.

in $\boldsymbol{n}_1(l)$ can be obtained by comparing $\widetilde{\boldsymbol{x}}_{\mathrm{F}}(l)$ to a threshold E_{TH}, as shown in (18). For the lth block, let the index vector obtained from the threshold estimation formulated in (18) be $\boldsymbol{c}_{\mathrm{detect}}(l)$. We can show that when $\|\boldsymbol{c}_{\mathrm{detect}}(l)\|_0 = 0$, CIS is not required for this block, since no impairments can be estimated. By contrast, when we have $\|\boldsymbol{c}_{\mathrm{detect}}(l)\|_0 \neq 0$, CIS is indeed required for estimating the sparse vector $\boldsymbol{n}_1(l)$ from the measurements $\boldsymbol{y}_{\mathrm{F}}(l)$ formulated in (23). In this case, the mapping matrix $\boldsymbol{\Theta}_S$, which is related to the indices of the impairments to be estimated, can be obtained with the aid of $\mathcal{I}_S$, where $\mathcal{I}_S = Supp\{\boldsymbol{c}_{\mathrm{detect}}(l)\}$. Then, the corresponding values in $\widetilde{\boldsymbol{n}}_1(l)$ can be obtained by solving the correlation estimation problem of

$$\hat{\boldsymbol{n}}_1(l) = \arg\min_{\boldsymbol{n}_1(l)} \left\{ \|\boldsymbol{y}_{\mathrm{p}}(l) - \boldsymbol{A}\boldsymbol{n}_1(l)\|_2 \right\}, \tag{32}$$

which can be solved by following the least square approach formulated as $\hat{\boldsymbol{n}}_1(l) = \boldsymbol{\Theta}_S\left[\boldsymbol{\Theta}_S^{T}\boldsymbol{A}^{H}\boldsymbol{y}_{\mathrm{p}}(l)\right]$. Finally, we can show that the estimation performance of CIS is dependent on both the threshold E_{TH} and on the mutual coherence μ of $\boldsymbol{A}$, as detailed in Section III-A and Section IV-B.

After the estimation of $\hat{\boldsymbol{n}}_1(l)$, we can carry out the noise cancellation and form the decision variables for the lth block of received data symbols

IEEE Access
The journal for rapid open access publishing

Algorithm 2 CIS-Assisted Symbol Detector

Require: $\boldsymbol{\mathcal{F}}_M^H, \widetilde{\boldsymbol{x}}_{\mathrm{F}}(l), \mathcal{I}_{\mathrm{p}}, \mathcal{I}_{\mathrm{d}}$;

CIS :
Derive the index indicator vector $\boldsymbol{c}_{\mathrm{detect}}(l)$ using (18);
if $\|\boldsymbol{c}_{\mathrm{detect}}(l)\|_0 = 0$ **then**
  exit
else
  Form matrix $\boldsymbol{\Theta}_{\mathrm{p}}^T$ from $\mathcal{I}_{\mathrm{p}}$;
  Calculate $\boldsymbol{A} = \boldsymbol{\Theta}_{\mathrm{p}}^T \boldsymbol{\mathcal{F}}_M^H$ and then $\boldsymbol{y}_{\mathrm{p}}(l) = \boldsymbol{A}\widetilde{\boldsymbol{x}}_{\mathrm{F}}(l)$ based on (23);
  Set $\mathcal{I}_S = Supp\{\boldsymbol{c}_{\mathrm{detect}}(l)\}$;
  Form a matrix $\boldsymbol{\Theta}_S^T$ based on $\mathcal{I}_S$;
  Find the estimation $\hat{\boldsymbol{n}}_1(l) = \boldsymbol{\Theta}_S \left[\boldsymbol{\Theta}_S^T \boldsymbol{A}^H \boldsymbol{y}_{\mathrm{p}}(l)\right]$ based on (32);
end if
Symbol Detection
Form a matrix $\boldsymbol{\Theta}_{\mathrm{d}}^T$ based on $\mathcal{I}_{\mathrm{d}}$;
Calculate $\widetilde{\boldsymbol{x}}_{\mathrm{d}}(l) = \boldsymbol{\Theta}_{\mathrm{d}}^T \boldsymbol{\mathcal{F}}_M^H (\widetilde{\boldsymbol{x}}_{\mathrm{F}}(l) - \hat{\boldsymbol{n}}_1(l))$ as shown in (33);
for $l = 0 \to L_M - 1$ **do**
  for $m = 0 \to M - 1$ **do**
    Detect $\hat{x}_{\mathrm{d}}(m, l)$ according to

$$\hat{x}_{\mathrm{d}}(m,l) = \underset{x_{\mathrm{d}}(m,l)\in\mathcal{A}}{\arg\min} \|\widetilde{x}_{\mathrm{d}}(m,l) - x_{\mathrm{d}}(m,l)\|^2,$$

    as shown in (34);
  end for
end for
return $\hat{\boldsymbol{x}}_{\mathrm{d}}(l)$.

as follows:

$$\begin{aligned}\widetilde{\boldsymbol{x}}_{\mathrm{d}}(l) &= \boldsymbol{\Theta}_{\mathrm{d}}^T \boldsymbol{\mathcal{F}}_M^H \left[\widetilde{\boldsymbol{x}}_{\mathrm{F}}(l) - \hat{\boldsymbol{n}}_1(l)\right] \\ &= \boldsymbol{\Theta}_{\mathrm{d}}^T \boldsymbol{\mathcal{F}}_M^H \left[\boldsymbol{x}_{\mathrm{F}}(l) + \boldsymbol{g}_{\mathrm{F}}(l) + \boldsymbol{n}_0(l) + \boldsymbol{n}_1(l) - \hat{\boldsymbol{n}}_1(l)\right] \\ &= \boldsymbol{\Theta}_{\mathrm{d}}^T \boldsymbol{\mathcal{F}}_M^H \boldsymbol{\mathcal{F}}_M \boldsymbol{\Theta}_{\mathrm{d}} \boldsymbol{x}_{\mathrm{d}}(l) + \boldsymbol{\Theta}_{\mathrm{d}}^T \boldsymbol{\mathcal{F}}_M^H \left[\boldsymbol{g}_{\mathrm{F}}(l) + \boldsymbol{n}_0(l) + \boldsymbol{e}_1(l)\right] \\ &= \boldsymbol{x}_{\mathrm{d}}(l) + \boldsymbol{n}_{\mathrm{d}0}(l), \end{aligned} \tag{33}$$

where, for simplicity, we defined $\boldsymbol{n}_{\mathrm{d}0}(l) = \boldsymbol{\Theta}_{\mathrm{d}}^T \boldsymbol{\mathcal{F}}_M^H [\boldsymbol{g}_{\mathrm{F}}(l) + \boldsymbol{n}_0(l) + \boldsymbol{e}_1(l)]$, with $\boldsymbol{e}_1(l) = \boldsymbol{n}_1(l) - \hat{\boldsymbol{n}}_1(l)$ representing the estimation error of CIS. Note that when M is sufficient large, the impairment $\boldsymbol{n}_{\mathrm{d}0}(l)$ can be approximated by a Gaussian vector. Assuming that data symbols in $\mathcal{A}$ are equiprobable, each transmitted symbol can be detected by applying the maximum-likelihood (ML) rule as

$$\hat{x}_{\mathrm{d}}(m,l) = \underset{x_{\mathrm{d}}(m,l)\in\mathcal{A}}{\arg\min} \|\widetilde{x}_{\mathrm{d}}(m,l) - x_{\mathrm{d}}(m,l)\|^2, \tag{34}$$

for $m = 0, 1, \ldots, M_{\mathrm{d}} - 1$ and $l = 0, 1, \ldots, L_M - 1$.

Based on the above analysis, the proposed CIS-assisted symbol detector is summarized in Algorithm 2. It should be noted that the computational cost related to the mapping matrices, including $\boldsymbol{\Theta}_{\mathrm{d}}$, $\boldsymbol{\Theta}_{\mathrm{p}}$, $\boldsymbol{\Theta}_S$, can be neglected since in practice, they only represent row or column selection operations. Hence, when the CIS aided impairment estimation is activated, the corresponding computational complexity is on the order of $\mathcal{O}(k_S M_{\mathrm{p}}^2)$, where $k_S = \|\boldsymbol{c}_{\mathrm{detect}}(l)\|_0$ characterizes the grade of sparsity for the vector to be estimated. The computational complexity of the symbol detection process shown in Algorithm 2 is on the order of $\mathcal{O}(QM_{\mathrm{d}})$. Thus, it can be readily shown that the total complexity of Algorithm 2 is rather low, since the values of k_S and M_{p} are significantly lower than M.

V. SIMULATION RESULTS

In this section, simulation results are provided for characterizing the achievable performance of the proposed IDFFT aided system. Firstly, let us consider the system setup and the parameters used in our simulations, which are summarized in Table 1.

TABLE 1. Parameters for all simulations.

Channel	$\lvert h_{\mathrm{F}}(m)\rvert \sim$Log-$\mathcal{N}(\Omega_H(m), \sigma_H^2(m))$ $\Omega_H(m) = 0.537m^{-0.496} + 0.001512$ [6] $\sigma_H(m) = 0.445m^{-0.256} - 0.025574$ [6] Phase$(h_{\mathrm{F}}(m)) \sim$ Unif$(-\pi, \pi)$
Noise	$\Omega_0 = 15.2$ ms, $\Lambda_{\mathrm{T}} = -30$ dB $\Lambda_{\mathrm{P}} = 50$ dB
System	$M = 256$, $L_{\mathrm{cp}} = 60$, $\Delta t = 31.25$ ns $L_\Pi = L_M M$, $a_\Pi = 0.5$, $\varepsilon_\Pi = \sqrt{a_\Pi L_M} + 1$

A. SYSTEM SETUP AND PARAMETERS

In our simulations, we assume an OFDM system employing $M = 256$ subcarriers and operated in the 1.813-17.813 MHz frequency range. The subcarrier spacing is 62.5 kHz. We consider the scenario of the power grid in Europe, where the mains frequency is 50 Hz. Based on the measurement results of [5], the PLC channel is assumed to be time-invariant within a duration of about 600 μs. In this case, we assume that a total of $L_H = 50$ blocks of OFDM symbols are transmitted during each time-invariant channel segment. For each time-invariant duration, the FDCHTF is generated based on Section II-C and the corresponding parameters are given in Table 1. The average attenuation of the PLC channel is assumed to be constant. In our IDFFT aided system, the CP length is chosen to be $L_{\mathrm{cp}} = 60$. For the background and asynchronous impulsive noise, the noise model described in Section II-D is considered in conjunction with the parameters listed in Table 1. In particular, the power spectral density (PSD) level of the background noise is chosen to be -110 dBm/kHz. Furthermore, as shown by measurement results of [7], the power ratio between the asynchronous impulsive noise and the background noise is typically $\Lambda_{\mathrm{P}} = 50$ dB. For reasons of statistical relevance, all simulation results are obtained from the average of the results obtained in a duration of 10 seconds. Throughout this section, the SNR per bit denoted as γ_0 is the ratio between the transmitted power per bit and the power of background noise.

B. PERFORMANCE RESULTS

In Fig. 4, the BER performance of the proposed IDFFT aided system and of the conventional OFDM system is compared,

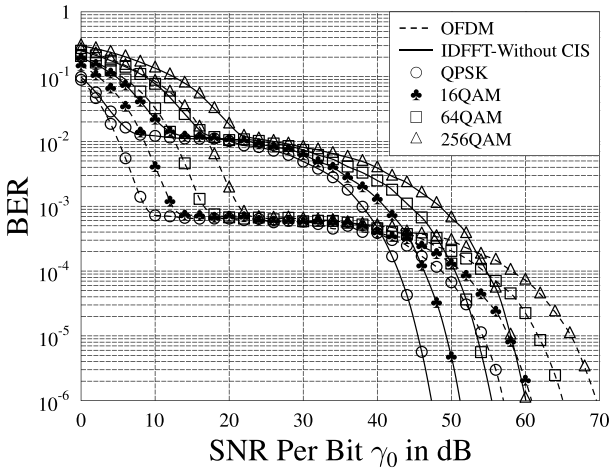

FIGURE 4. Performance comparison between the IDFFT aided PLC system without CIS and the conventional OFDM system, when communicating over the dispersive PLC channel contaminated by both background noise and asynchronous impulsive noise. The parameters are $L_\Pi = 50 \times M$, $\Lambda_T = -30$ dB, $\Lambda_P = 50$ dB.

when communicating over indoor PLC channels contaminated by both the background noise and the impulsive noise. In this figure, four signal constellations are considered, which are QPSK, 16QAM, 64QAM and 256QAM. The parameters used for characterizing the impulsive noise are chosen to be $\Lambda_T = -30$ dB and $\Lambda_P = 50$ dB. The IDFFT aided system employs the 2D interleaver size of $L_\Pi = 50 \times M$, i.e., $L_M = 50$. Furthermore, in Fig. 4, the CIS-assisted impairment estimation is not employed and hence no pilots are used. From the results of Fig. 4, we observe that the IDFFT aided system outperforms the conventional OFDM system in the relatively high SNR range, which becomes more pronounced, as γ_0 increases. This observation can be explained as follows. In the IDFFT aided system, there are two types of spreading, namely the FD spreading by the IFFT and the 2D spreading by the interleaver Π, as seen in Fig. 2. Because of these two spreading schemes, every data symbol is conveyed by all the L_M blocks of transmitted signals, as shown in (3). By contrast, every data symbol is only conveyed by a single block of signals in the conventional OFDM system, since its transmitter can only generate the FD spreading effect by the IFFT operation. In principle, the detection performance is mainly affected by the FDCHTF and the impulsive noise, when the SNR is high. In this case, in the IDFFT aided system, the effect of both the FDCHTF and of the impulsive noise is distributed (or averaged) over all the L_M blocks of signals, hence resulting in a steep decay of the average BER curve, as the SNR increases. By contrast, in conventional OFDM systems, the above-mentioned effect is only distributed over a single block of signals, which has a substantial impact on the average error probability. From another angle, we can say that the IDFFT aided system achieves a higher multipath-induced diversity gain than the conventional OFDM system. However, we should note that in the low SNR range, the BER performance is dominated by the background noise. The IFFT-induced spreading effect may introduce more errors for the IDFFT aided system, since in this case, more blocks are impaired by impulsive noise. Consequently, in the low SNR range, the conventional OFDM system achieves a better BER performance than the IDFFT aided system.

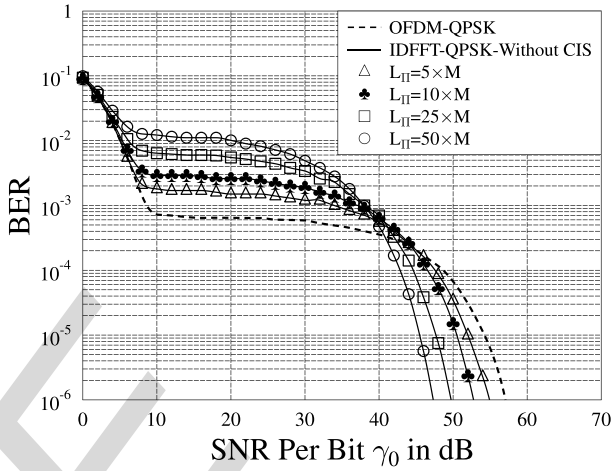

FIGURE 5. BER performance of the IDFFT PLC system using QPSK and different interleaver sizes L_Π, when communicating over the PLC channel experiencing both asynchronous impulsive noise and background noise.

Fig. 5 shows the effect of the interleaver's size on the BER performance of our IDFFT aided system using QPSK modulation, when communicating over the indoor PLC channels experiencing both background noise and asynchronous impulsive noise. In this figure, the size of the 2D interleaver Π of Fig. 3 is chosen to be $L_\Pi = L_M M$, where $L_M = 5$, 10, 25 or 50. Again, in this figure, no CIS-assisted impairment estimation is considered. Fig. 5 shows that in the high-SNR region, increasing the size of the interleaver is capable of improving the attainable BER performance. However, in the low-to-medium SNR region, the BER performance degrades, as the interleaver size increases. This observation can be explained with the aid of (13). By substituting the spreading factor ε_Π shown in Table 1 into (13), it can be readily shown that the higher the value of L_M, the high the dispersion capability of the 2D interleaver Π becomes. Hence, when the SNR is high enough, the spreading effect of the 2D interleaver Π becomes beneficial, since all subcarriers are only marginally contaminated. By contrast, when the SNR is lower than a certain value, such as $\gamma_0 = 40$ dB in Fig. 5, the 2D spreading effect of Π degrades the attainable BER performance, since after de-interleaving, more errors are introduced into those specific blocks that were originally not impaired by impulsive noise. It should be noted that when choosing the size of the interleaver Π, a tradeoff has to be struck between the performance gain attained and the time delay imposed.

In Fig. 6, we investigate the effects of sparsity level $k(l)$ associated with the impairment vector $\boldsymbol{n}_1(l)$ defined in (21) by varying both the threshold E_{TH} and the interleaver size L_Π. In this figure, the IDFFT system operates at the SNR per

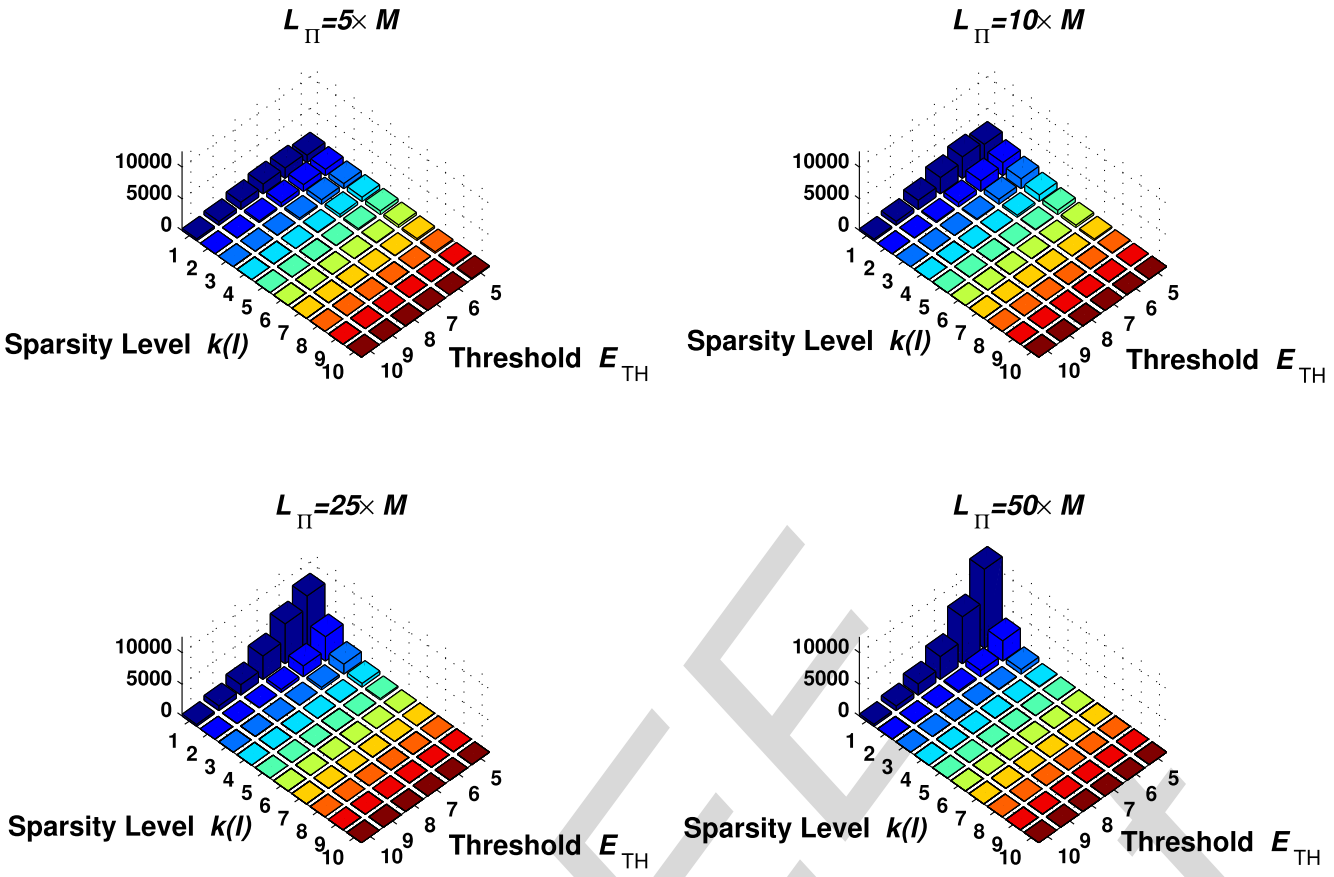

FIGURE 6. Sparsity level $k(l)$ associated with the impairment vector $\boldsymbol{n}_1(l)$ versus the threshold E_{TH}, for the IDFFT aided system using QPSK modulation communicating over dispersive PLC channels contaminated by both asynchronous impulsive noise and background noise. The SNR per bit is $\gamma_0 = 35$ dB.

bit value of $\gamma_0 = 35$ dB without employing CIS-assisted impairment estimation. Moreover, in order to meet the PAPR constraint of (16), the threshold is set to $E_{\text{TH}} \geq 5$. As depicted in Fig. 6, when the interleaver size L_Π increases from $L_M = 5M$ to $L_M = 50M$, the sparsity level distribution of the impairment vector $\boldsymbol{n}_1(l)$ becomes more "peaky" around the low values of $k(l)$ and E_{TH}. Furthermore, when the interleaver size L_Π is fixed, the higher the threshold E_{TH}, the more sparse the impairment vector $\boldsymbol{n}_1(l)$ becomes. These observations confirm our analysis in Section III-A, namely that the sparsity condition of (21) can be satisfied with the aid of the 2D interleaver Π relying on the threshold estimation of (18). Therefore, it is indeed possible to estimate the impairment vector $\boldsymbol{n}_1(l)$ by exploiting the principle of CS.

In Fig. 7 and Fig. 8, we investigate the BER performance of the CIS-assisted IDFFT aided system using QPSK upon varying the number of pilots, when communicating over the dispersive PLC channels contaminated by both impulsive noise and background noise. In this figure, the interleaver size is chosen to be $L_\Pi = 50 \times M$. Firstly, as seen in Fig. 7, in comparison to the equi-spaced pilots, which is usually used in the conventional pilot-assisted estimation scheme, Algorithm 1 provides a significantly reduced mutual coherence of the measurement matrix $\boldsymbol{A}$. Hence, as stated in Section IV-B, when an estimation problem is solved with the

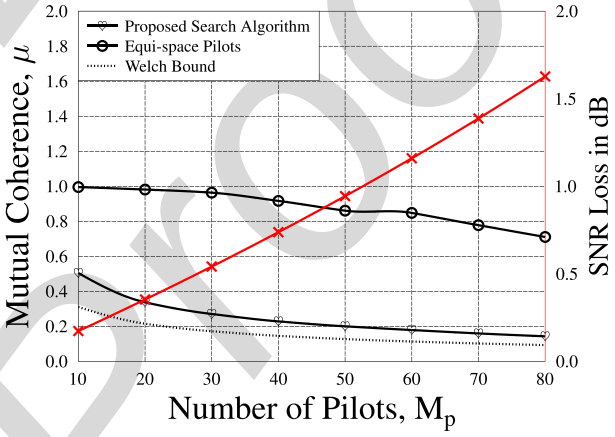

FIGURE 7. Mutual coherence μ and SNR loss versus the number of pilots M_p, when our proposed search algorithm is applied for constructing the measurement matrix $\boldsymbol{A}$ of size $M_p \times 256$.

aid of CS, the performance achieved by our proposed design of the pilot positions should be better than that achieved by the equi-spaced scheme. Secondly, Fig. 7 shows that upon increasing the number of pilots, a measurement matrix $\boldsymbol{A}$ having a lower mutual coherence can be obtained, which implies that a better overall performance can be attained. This inference can be verified by the simulation results shown in Fig. 8.

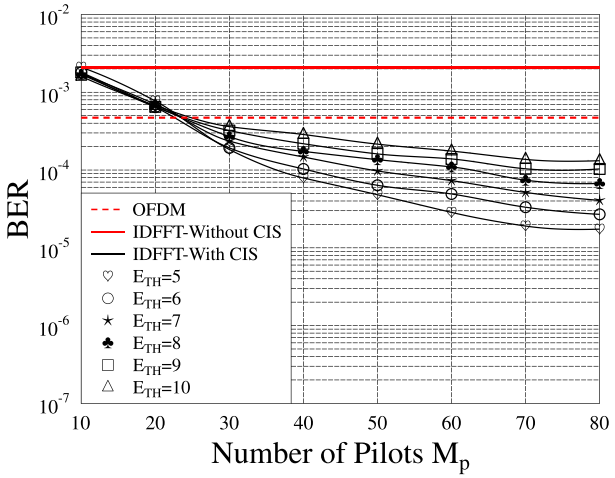

FIGURE 8. BER versus the number of pilots M_p, for the CIS-assisted IDFFT aided system using QPSK modulation for communicating over dispersive PLC channels contaminated by both asynchronous impulsive noise and background noise. The parameters are $L_\Pi = 50 \times M$, $\gamma_0 = 35$ dB.

As observed in Fig. 8, when the number of pilots increases, the BER performance of the CIS-assisted IDFFT system improves. Thirdly, the performance improvements achieved by the CIS-assisted detection of Section IV are achieved at the cost of an SNR loss imposed by using a higher proportion of pilots, as seen in Fig. 7. This tradeoff is confirmed by the simulation results of Fig. 8. As seen in Fig. 8, when the number of pilots increases, the attainable performance gain becomes more marginal. This implies that for a high proportion of pilots, the performance gain achieved by the CIS-assisted detection becomes saturated. Thus, as inferred from Fig. 7 and Fig. 8, there is an optimal value for M_p, which allows our proposed CIS-assisted detection algorithm to attain its best performance. Fourthly, as observed from Fig. 8, for a given number of pilots, the achievable performance gain is reduced, as the threshold E_{TH} is increased. This observation can be explained with the aid of Fig. 6 and (18). When the threshold E_{TH} is increased, the number of impairment events detected by the threshold-based estimator of (18) is reduced. Hence, the attainable performance gain becomes limited. Finally, we can infer from both Fig. 4 and Fig. 8 that the BER performance can be significantly improved by our CIS-assisted IDFFT aided system in comparison to the conventional OFDM system.

VI. CONCLUSIONS

In this paper, CIS-assisted IDFFT aided systems have been proposed for broadband indoor PLCs, in order to mitigate the deleterious effects of both the multipath fading and asynchronous impulsive noise. In this section, we summarize the basic design guidelines of our CIS-assisted IDFFT aided system.

- The 2D interleaver of the proposed CIS-assisted IDFFT aided system has to be carefully designed in order to disperse the impulsive noise bursts at the cost of the lowest possible time delay.
- The design of pilot symbols also commands special attention in order to facilitate the accurate estimation and efficient mitigation of asynchronous impulsive noise, because the specific position and number of pilots critically affects the CS-based estimation performance. Hence, the proposed search algorithm is recommended for designing the positions of the pilots in an offline manner. The number of pilots has to be optimized for striking a flexible tradeoff between the performance gain attained and the effective transmission rate reduction imposed by the pilot-overhead.
- Finally, based on the 2D interleaver and pilot design, the proposed CIS-assisted symbol detector is advocated, which has been shown to be capable of significantly improving the attainable system performance in comparison to the conventional OFDM system. Upon following these design guidelines, the computational complexity of the proposed CIS-assisted symbol detector remains low. The extra complexity is mainly contributed by the additional FFT and IFFT operations.

In order to further improve the attainable system performance, error correction coded turbo receivers will be applied to the CIS-assisted IDFFT system, which will be our future work.

REFERENCES

[1] L. Hanzo, H. Haas, S. Imre, D. O'Brien, M. Rupp, and L. Gyongyosi, "Wireless myths, realities, and futures: From 3G/4G to optical and quantum wireless," *Proc. IEEE*, vol. 100, pp. 1853–1888, May 2012. AQ:1
[2] F. J. Canete, J. A. Cortes, L. Diez, and J. T. Entrambasaguas, "Modeling and evaluation of the indoor power line transmission medium," *IEEE Commun. Mag.*, vol. 41, no. 4, pp. 41–47, Apr. 2003.
[3] H. Hrasnica, A. Haidine, and R. Lehnert, *Broadband Powerline Communications: Network Design*. New York, NY, USA: Wiley, 2005.
[4] M. Zimmermann and K. Dostert, "A multipath model for the powerline channel," *IEEE Trans. Commun.*, vol. 50, no. 4, pp. 553–559, Apr. 2002.
[5] F. J. C. Corripio, J. A. C. Arrabal, L. D. del Rio, and J. T. E. Munoz, "Analysis of the cyclic short-term variation of indoor power line channels," *IEEE J. Sel. Areas Commun.*, vol. 24, no. 7, pp. 1327–1338, Jul. 2006.
[6] A. M. Tonello, F. Versolatto, and A. Pittolo, "In-home power line communication channel: Statistical characterization," *IEEE Trans. Commun.*, vol. 62, no. 6, pp. 2096–2106, Jun. 2014.
[7] M. Zimmermann and K. Dostert, "Analysis and modeling of impulsive noise in broad-band powerline communications," *IEEE Trans. Electromagn. Compat.*, vol. 44, no. 1, pp. 249–258, Feb. 2002.
[8] H. Meng, Y. L. Guan, and S. Chen, "Modeling and analysis of noise effects on broadband power-line communications," *IEEE Trans. Power Del.*, vol. 20, no. 2, pp. 630–637, Apr. 2005.
[9] J. A. Cortés, L. Díez, F. J. Cañete, and J. J. Sánchez-Martínez, "Analysis of the indoor broadband power-line noise scenario," *IEEE Trans. Electromagn. Compat.*, vol. 52, no. 4, pp. 849–858, Nov. 2010.
[10] K. L. Blackard, T. S. Rappaport, and C. W. Bostian, "Measurements and models of radio frequency impulsive noise for indoor wireless communications," *IEEE J. Sel. Areas Commun.*, vol. 11, no. 7, pp. 991–1001, Sep. 1993.
[11] L. L. Hanzo, M. Münster, B. Choi, and T. Keller, *OFDM and MC-CDMA for Broadband Multi-User Communications, WLANs and Broadcasting*. New York, NY, USA: Wiley, May 2003.
[12] L.-L. Yang, *Multicarrier Communications*. New York, NY, USA: Wiley, 2009.
[13] *IEEE Standard for Broadband Over Power Line Networks: Medium Access Control and Physical Layer Specifications*, IEEE Standard 1901-2010, 2010, pp. 1–1586.
[14] *Unified High-Speed Wireline-Based Home Networking Transceivers—System Architecture and Physical Layer Specification*, document ITRG 9960, 2011. AQ:2

[15] *HomePlug AV2 White Paper. HomePlug Powerline Alliance*. [Online]. Available: http://www.homeplug.org/

[16] H. A. Suraweera, C. Chai, J. Shentu, and J. Armstrong, "Analysis of impulse noise mitigation techniques for digital television systems," in *Proc. 8th Int. OFDM Workshop*, Sep. 2003, pp. 172–176.

[17] S. V. Zhidkov, "Analysis and comparison of several simple impulsive noise mitigation schemes for OFDM receivers," *IEEE Trans. Commun.*, vol. 56, no. 1, pp. 5–9, Jan. 2008.

[18] C.-H. Yih, "Iterative interference cancellation for OFDM signals with blanking nonlinearity in impulsive noise channels," *IEEE Signal Process. Lett.*, vol. 19, no. 3, pp. 147–150, Mar. 2012.

[19] N. Andreadou and A. M. Tonello, "On the mitigation of impulsive noise in power-line communications with LT codes," *IEEE Trans. Power Del.*, vol. 28, no. 3, pp. 1483–1490, Jul. 2013.

[20] N. Andreadou and F.-N. Pavlidou, "Mitigation of impulsive noise effect on the PLC channel with QC–LDPC codes as the outer coding scheme," *IEEE Trans. Power Del.*, vol. 25, no. 3, pp. 1440–1449, Jul. 2010.

[21] J. Haring and A. J. H. Vinck, "Iterative decoding of codes over complex numbers for impulsive noise channels," *IEEE Trans. Inf. Theory*, vol. 49, no. 5, pp. 1251–1260, May 2003.

[22] J. Lin, M. Nassar, and B. L. Evans, "Impulsive noise mitigation in power-line communications using sparse Bayesian learning," *IEEE J. Sel. Areas Commun.*, vol. 31, no. 7, pp. 1172–1183, Jul. 2013.

[23] S. S. Chen, D. L. Donoho, and M. A. Saunders, "Atomic decomposition by basis pursuit," *SIAM J. Sci. Comput.*, vol. 20, no. 1, pp. 33–61, 1999.

[24] R. Tibshirani, "Regression shrinkage and selection via the lasso," *J. Roy. Stat. Soc. Ser. B*, vol. 58, no. 1, pp. 267–288, 1996.

[25] E. Candes and T. Tao, "The Dantzig selector: Statistical estimation when p is much larger than n," *Ann. Statist.*, vol. 35, no. 6, pp. 2313–2351, Dec. 2007.

[26] J. A. Tropp, "Greed is good: Algorithmic results for sparse approximation," *IEEE Trans. Inf. Theory*, vol. 50, no. 10, pp. 2231–2242, Oct. 2004.

[27] D. Needell and J. A. Tropp, "CoSaMP: Iterative signal recovery from incomplete and inaccurate samples," *Appl. Comput. Harmon. Anal.*, vol. 26, no. 3, pp. 301–321, May 2009.

[28] T. Blumensath and M. E. Davies, "Iterative hard thresholding for compressed sensing," *Appl. Comput. Harmon. Anal.*, vol. 27, no. 3, pp. 265–274, Nov. 2009.

[29] D. L. Donoho, "Compressed sensing," *IEEE Trans. Inf. Theory*, vol. 52, no. 4, pp. 1289–1306, Apr. 2006.

[30] W. U. Bajwa, J. Haupt, A. M. Sayeed, and R. Nowak, "Compressed channel sensing: A new approach to estimating sparse multipath channels," *Proc. IEEE*, vol. 98, no. 6, pp. 1058–1076, Jun. 2010.

[31] A. Gomaa and N. Al-Dhahir, "A sparsity-aware approach for NBI estimation in MIMO-OFDM," *IEEE Trans. Wireless Commun.*, vol. 10, no. 6, pp. 1854–1862, Jun. 2011.

[32] Z. Tian and G. B. Giannakis, "Compressed sensing for wideband cognitive radios," in *Proc. IEEE Int. Conf. Acoust., Speech Signal Process. (ICASSP)*, vol. 4. Apr. 2007, pp. IV-1357–IV-1360.

[33] G. Caire, T. Y. Al-Naffouri, and A. K. Narayanan, "Impulse noise cancellation in OFDM: An application of compressed sensing," in *Proc. IEEE Int. Symp. Inf. Theory (ISIT)*, Jul. 2008, pp. 1293–1297.

[34] L. Lampe, "Bursty impulse noise detection by compressed sensing," in *Proc. IEEE Int. Symp. Power Line Commun. Appl. (ISPLC)*, Apr. 2011, pp. 29–34.

[35] U. Sorger, I. De Broeck, and M. Schnell, "Interleaved FDMA—A new spread-spectrum multiple-access scheme," in *Proc. IEEE Int. Rec. Conf. Commun. (ICC)*, vol. 2. Jun. 1998, pp. 1013–1017.

[36] Z. Liu, "Maximum diversity in single-carrier frequency-domain equalization," *IEEE Trans. Inf. Theory*, vol. 51, no. 8, pp. 2937–2940, Aug. 2005.

[37] Channel Model Sub-committee of P1901, "Electrical network and topology channel and noise model," Tech. Rep. P1901-10-0356-00, Sep. 2010.

[38] FP7 Theme 3 ICT-213311 OMEGA, "PLC channel characterization and modelling," Tech. Rep., Dec. 2008.

[39] D. Divsalar and F. Pollara, "Turbo codes for PCS applications," in *Proc. IEEE Int. Conf. Commun. (ICC)*, vol. 1. Seattle, WA, USA, Jun. 1995, pp. 54–59.

[40] S. Dolinar and D. Divsalar, "Weight distributions for turbo codes using random and nonrandom permutations," Jet Propulsion Lab., Pasadena, CA, USA, Tech. Rep. 42-122, Aug. 1995.

[41] H. R. Sadjadpour, N. J. A. Sloane, M. Salehi, and G. Nebe, "Interleaver design for turbo codes," *IEEE J. Sel. Areas Commun.*, vol. 19, no. 5, pp. 831–837, May 2001.

[42] J. Sun and O. Y. Takeshita, "Interleavers for turbo codes using permutation polynomials over integer rings," *IEEE Trans. Inf. Theory*, vol. 51, no. 1, pp. 101–119, Jan. 2005.

[43] T. Jiang, M. Guizani, H.-H. Chen, W. Xiang, and Y. Wu, "Derivation of PAPR distribution for OFDM wireless systems based on extreme value theory," *IEEE Trans. Wireless Commun.*, vol. 7, no. 4, pp. 1298–1305, Apr. 2008.

[44] H. V. Poor and S. Verdu, "Probability of error in MMSE multiuser detection," *IEEE Trans. Inf. Theory*, vol. 43, no. 3, pp. 858–871, May 1997.

[45] Y. Jiang, M. K. Varanasi, and J. Li, "Performance analysis of ZF and MMSE equalizers for MIMO systems: An in-depth study of the high SNR regime," *IEEE Trans. Inf. Theory*, vol. 57, no. 4, pp. 2008–2026, Apr. 2011.

[46] D. L. Donoho, M. Elad, and V. N. Temlyakov, "Stable recovery of sparse overcomplete representations in the presence of noise," *IEEE Trans. Inf. Theory*, vol. 52, no. 1, pp. 6–18, Jan. 2006.

[47] T. T. Cai and L. Wang, "Orthogonal matching pursuit for sparse signal recovery with noise," *IEEE Trans. Inf. Theory*, vol. 57, no. 7, pp. 4680–4688, Jul. 2011.

[48] B. K. Natarajan, "Sparse approximate solutions to linear systems," *SIAM J. Comput.*, vol. 24, no. 2, pp. 227–234, 1995.

[49] S. Boyd and L. Vandenberghe, *Convex Optimization*. Cambridge, U.K.: Cambridge Univ. Press, 2004.

[50] D. L. Donoho and X. Huo, "Uncertainty principles and ideal atomic decomposition," *IEEE Trans. Inf. Theory*, vol. 47, no. 7, pp. 2845–2862, Nov. 2001.

[51] E. J. Candès and T. Tao, "Decoding by linear programming," *IEEE Trans. Inf. Theory*, vol. 51, no. 12, pp. 4203–4215, Dec. 2005.

[52] A. M. Tillmann and M. E. Pfetsch, "The computational complexity of the restricted isometry property, the nullspace property, and related concepts in compressed sensing," *IEEE Trans. Inf. Theory*, vol. 60, no. 2, pp. 1248–1259, Feb. 2014.

[53] L. Welch, "Lower bounds on the maximum cross correlation of signals (Corresp.)," *IEEE Trans. Inf. Theory*, vol. 20, no. 3, pp. 397–399, May 1974.

[54] D. V. Sarwate, *Meeting the Welch Bound With Equality* (Discrete Mathematics and Theoretical Computer Science). New York, NY, USA: Springer-Verlag, 1999.

[55] M. A. Sustik, J. A. Tropp, I. S. Dhillon, and R. W. Heath, Jr., "On the existence of equiangular tight frames," *Linear Algebra Appl.*, vol. 426, nos. 2–3, pp. 619–635, Oct. 2007.

[56] N. Y. Yu, "A construction of codebooks associated with binary sequences," *IEEE Trans. Inf. Theory*, vol. 58, no. 8, pp. 5522–5533, Aug. 2012.

[57] D. J. Love, R. W. Heath, and T. Strohmer, "Grassmannian beamforming for multiple-input multiple-output wireless systems," *IEEE Trans. Inf. Theory*, vol. 49, no. 10, pp. 2735–2747, Oct. 2003.

[58] P. Xia, S. Zhou, and G. B. Giannakis, "Achieving the Welch bound with difference sets," *IEEE Trans. Inf. Theory*, vol. 51, no. 5, pp. 1900–1907, May 2005.

[59] A. Medra and T. N. Davidson, "Flexible codebook design for limited feedback systems via sequential smooth optimization on the Grassmannian manifold," *IEEE Trans. Signal Process.*, vol. 62, no. 5, pp. 1305–1318, Mar. 2014.

HONGMING ZHANG (S'15) received the B.Eng. (Hons.) degree in telecommunications from the Nanjing University of Aeronautics and Astronautic and the City University London, in 2011, and the M.Sc. degree in wireless communications from the University of Southampton, in 2012, where he is currently pursuing the Ph.D. degree. His research interests include power line communications, compressed sensing, and the design of communications systems.

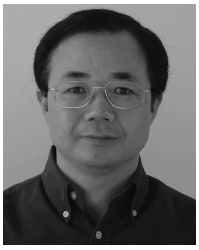

LIE-LIANG YANG (M'98–SM'02–F'15) received the B.Eng. degree in communications engineering from Shanghai Tiedao University, Shanghai, China, in 1988, and the M.Eng. and Ph.D. degrees in communications and electronics from Northern Jiaotong University, Beijing, China, in 1991 and 1997, respectively. In 1997, he was a Visiting Scientist with the Institute of Radio Engineering and Electronics, Academy of Sciences of the Czech Republic. Since 1997, he has been with the University of Southampton, U.K., where he is currently a Professor of Wireless Communications with the School of Electronics and Computer Science. His research has covered a wide range of topics in wireless communications, networking, and signal processing. He has authored over 300 research papers in journals and conference proceedings, authored/co-authored three books, and also published several book chapters. He is a fellow of IET, and served as an Associate Editor of the IEEE TRANSACTIONS ON VEHICULAR TECHNOLOGY and the *Journal of Communications and Networks*. He is currently an Associate Editor of the IEEE ACCESS and the *Security and Communication Networks* journal.

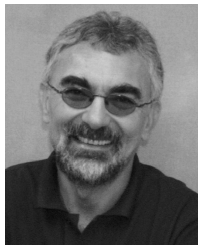

LAJOS HANZO received the D.Sc. degree in electronics in 1976, the Ph.D. degree in 1983, and the Doctor Honoris Causa degree from the Technical University of Budapest, in 2009. During his 35-year career in telecommunications, he has held various research and academic positions in Hungary, Germany, and the U.K. Since 1986, he has been with the School of Electronics and Computer Science, University of Southampton, U.K., as the Chair in Telecommunications. He has successfully supervised 80 Ph.D. students, co-authored 20 John Wiley/IEEE Press books in mobile radio communications totaling in excess of 10 000 pages, authored over 1500 research entries at the IEEE Xplore, acted as the TPC Chair and General Chair of the IEEE conferences, presented keynote lectures, and received a number of distinctions. He is directing 60 strong academic research teams, working on a range of research projects in the field of wireless multimedia communications sponsored by the industry, the Engineering and Physical Sciences Research Council, U.K., the European IST Program, and the Mobile Virtual Centre of Excellence, U.K. He is an enthusiastic supporter of industrial and academic liaison and offers a range of industrial courses. He is a fellow of the Royal Academy of Engineering, the Institution of Engineering and Technology, and the European Association for Signal Processing. He is also a Governor of the IEEE VTS. From 2008 to 2012, he was the Editor-in-Chief of the *IEEE Press* and a Chaired Professor with Tsinghua University, Beijing. His research is funded by the European Research Council's Senior Research Fellow Grant.

AUTHOR QUERIES

AQ:1 = Please provide the issue no. for ref. [1].
AQ:2 = Please confirm the document no. for ref. [14].
AQ:3 = Please confirm the title. Also provide the accessed date for ref. [15].
AQ:4 = Please confirm the author name, title, and report no. Also provide the organization name and organization location for ref. [37].
AQ:5 = Please confirm the author name, title, and year Also provide the organization name, organization location, and report no. for ref. [38].
AQ:6 = Please confirm the report no. for ref. [40].